CATEGORY
SPECIAL HANDLING
7

# TECHNICAL MEMORANDUM

CLASSIFICATION CHANGED

UNCLASSIFIED

X-513  TO

By Authority of $T.D.71-617$  Date $10/5/71$

TRANSONIC WIND-TUNNEL INVESTIGATION OF THE STATIC

LONGITUDINAL STABILITY AND PERFORMANCE CHARACTERISTICS

OF A SUPERSONIC FIGHTER-BOMBER AIRPLANE

By Arvo A. Luoma

Langley Research Center
Langley Field, Va.

Declassified by authority of NASA
Classification Change Notices No. 515
Dated ** 12/31/71

NATIONAL AERONAUTICS AND SPACE ADMINISTRATION

WASHINGTON                                             July 1961

NATIONAL AERONAUTICS AND SPACE ADMINISTRATION
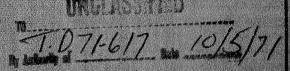
TECHNICAL MEMORANDUM X-513

TRANSONIC WIND-TUNNEL INVESTIGATION OF THE STATIC

LONGITUDINAL STABILITY AND PERFORMANCE CHARACTERISTICS

OF A SUPERSONIC FIGHTER-BOMBER AIRPLANE*

By Arvo A. Luoma

SUMMARY

An investigation of the longitudinal aerodynamic characteristics of various configurations of a 1/22-scale model of a supersonic fighter-bomber airplane has been made at Mach numbers from 0.60 to 1.20. All the configurations were tested with internal flow. All the tests were made at a horizontal-tail deflection of $-3^{\circ}$. Configurations included single-place and two-place canopies, short and long body noses, external stores, an afterbody bump for fuel storage, and exit-nozzle blisters based on the area rule.

The effect of configuration modifications on longitudinal stability and trim was small. Area-rule modifications showed some drag reductions at sonic and supersonic speeds. External stores caused substantial increases in drag.

INTRODUCTION

A proposed addition to a series of supersonic fighter-bomber aircraft was a two-place version with all-weather capability. Transonic and supersonic wind-tunnel tests of the performance and longitudinal and lateral stability characteristics of the two-place design were conducted for the purpose of checking the estimated aerodynamic characteristics. The results of an investigation at supersonic speeds in the Langley Unitary Plan wind tunnel of the aerodynamic characteristics of the single-place and two-place versions are presented in reference 1.

An investigation at transonic speeds of the longitudinal aerodynamic characteristics of a 1/22-scale model of the single-place and

two-place versions of the airplane was started in the Langley 8-foot
transonic tunnel and completed in the Langley 8-foot transonic pressure
tunnel. The results of this investigation are presented herein. These
results include information on the effect on performance and longitudinal
stability characteristics of two designs of a two-place canopy; a longer
body nose; wing-tip tanks, wing inboard tanks, and center-line tanks;
chaff dispensers; air-to-air missiles; an afterbody bump for fuel storage;
and exit-nozzle blisters based on the area rule. The tests were made at
Mach numbers from 0.60 to 1.20 through a maximum angle-of-attack range
which was approximately $-2°$ to $22°$ at the lower Mach numbers and approxi-
mately $-2°$ to $13°$ at the higher Mach numbers.

## SYMBOLS

The aerodynamic force and moment data are referred to the wind
axes, with the origin at the center-of-gravity location shown in fig-
ure 1. This location coincided with the 25-percent point of the mean
aerodynamic chord of the wing. The symbols used are defined as follows:

A           aspect ratio of wing, $\dfrac{b^2}{S}$

$A_e$          area of duct at duct exit (end of body)

$A_p$          projected area of duct inlet on plane perpendicular to
            reference line of body

b           span (projected) of wing

$C_D$          external-drag coefficient, $\dfrac{\text{External drag}}{q_\infty S}$

$C_{D,i}$        internal-drag coefficient, $\dfrac{w}{q_\infty S}\left(V_\infty - V_e \cos \alpha\right) - C_{p,e}\dfrac{A_e}{S}\cos \alpha$

$C_{D,o}$        external-drag coefficient at zero lift

$\dfrac{\Delta C_D}{\Delta C_L^2}$        drag-rise factor

$C_L$          lift coefficient, $\dfrac{\text{Lift}}{q_\infty S}$

$C_m$    pitching-moment coefficient, $\dfrac{\text{Pitching moment}}{q_\infty S \bar{c}}$

$C_{p,e}$    pressure coefficient of flow in duct at duct exit (end of body), $\dfrac{p_e - p_\infty}{q_\infty}$

$\bar{c}$    mean aerodynamic chord of wing, $\dfrac{2}{3} c_r \dfrac{1 + \lambda + \lambda^2}{1 + \lambda}$

$c_r$    root chord of wing, obtained by extending straight portions of leading and trailing edges of wing to plane of symmetry of model

$c_t$    nominal tip chord of wing, obtained by extending leading and trailing edges of wing to plane which is tangent to tip of wing, parallel to root chord of wing, and perpendicular to chord plane of wing

$(L/D)_{max}$    maximum value of lift-drag ratio

$M$    Mach number of undisturbed stream

$p_e$    static pressure of flow in duct at duct exit (end of body)

$p_\infty$    static pressure of undisturbed stream

$q_\infty$    dynamic pressure of undisturbed stream, $\dfrac{1}{2}\rho_\infty V_\infty{}^2$

$R$    Reynolds number, based on $\bar{c}$

$S$    area (projected) of wing, $\dfrac{b}{2}(c_r + c_t)$

$V_e$    velocity of flow in duct at duct exit (end of body)

$V_\infty$    velocity of undisturbed stream

$w$    mass flow in duct, $\rho_e V_e A_e$

$\dfrac{w}{w_\infty}$    mass-flow ratio based on projected area of inlet, $\dfrac{w}{\rho_\infty V_\infty A_p}$

$\alpha$    angle of attack, based on reference line of body

$\delta_h$      deflection of horizontal tail, determined by angle between plane of horizontal tail and reference line of body; positive when trailing edge is down

$\lambda$      taper ratio of wing, $c_t/c_r$

$\rho_e$      mass density of flow in duct at duct exit (end of body)

$\rho_\infty$      mass density of undisturbed stream

$$C_{L_\alpha} = \frac{dC_L}{d\alpha} \text{ per deg}$$

$$C_{m_{C_L}} = \frac{dC_m}{dC_L}$$

## APPARATUS

### Tunnels

The investigation was started in the Langley 8-foot transonic tunnel (8' TT) and completed in the Langley 8-foot transonic pressure tunnel (8' TPT). Both tunnels have slotted test sections that permit continuous testing through the transonic speed range. The 8-foot transonic tunnel has a dodecagonal test section with axial slots located at the vertices. The tunnel operates at a total pressure approximately equal to 1 atmosphere. A description of this tunnel and its airflow characteristics is given in reference 2. The 8-foot transonic pressure tunnel has a square cross section with axial slots in the top and bottom walls only. This tunnel can be operated over a range of total pressures, and the tunnel air is dried sufficiently to avoid condensation effects. Figures showing a typical model installation in the transonic pressure tunnel and representative axial Mach number distributions at the center of the test section of the transonic pressure tunnel are given in reference 3.

In both tunnels, angle-of-attack changes were made by rotating the model in a vertical plane. The axis of rotation was rearward of the model center-of-gravity location by 8.6 inches in the 8-foot transonic tunnel and by 28.5 inches in the 8-foot transonic pressure tunnel.

## Model

Description.- The model used in the present investigation was a sting-supported, 1/22-scale model of a supersonic fighter-bomber airplane. This airplane is turbojet powered and has wing-root air inlets. The wing and horizontal tail of the model had 45° of sweepback of the quarter-chord line. The vertical tail had 48° of sweepback at the leading edge. The airfoil sections (parallel to the body reference line) of the wing were NACA 65A005.5 at the 0.38-semispan station and NACA 65A003.7 at the tip. The model wing was built of steel. A three-view drawing and photographs of one of the model configurations are given in figures 1 and 2, respectively. The geometric characteristics of the model configurations are given in table I.

The model was designed for internal flow. Supersonic wing-root inlets were included on the model, and boundary-layer diverters were used with the inlets (fig. 2(d)). Ducts from the inlets led into a single duct which had an exit at the body base. The area of the inlet throat of the model in the present tests corresponded to the cruise condition, and is given in table I. The duct exit A shown in figure 3 was normally used in the present tests. Duct exits B and C were also used in determining the effect of duct exit area on mass flow and internal drag. The duct exit area could be changed by replacement of a bushing at the end of the body. The model was provided with inlet-duct bleeder ports for bypassing part of the internal flow, as indicated in figure 4. The bleeder ports were located on the body somewhat forward of the trailing edge of the wing. In the present investigation the bleeder ports were normally closed; a few tests were made with the bleeder ports half open.

Configuration identification.- Two body noses of different length and three canopies, a single-place canopy and two designs of a two-place canopy, were investigated. The body noses tested are shown in figure 5 and the canopies tested, in figure 6. The model configurations had various combinations of body noses and canopies and are identified herein as follows:

| Model configuration | Body nose | Canopy |
|---|---|---|
| 1 | Short | Single place |
| 2 | Short | Large two place |
| 3 | Long | Large two place |
| 4 | Long | Small two place |
| 5 | Long | Single place |

Each model configuration consisted of the combination of body, body-nose boom, canopy, wing (including air inlets), vertical tail (including antenna tip), horizontal tail, and ventral fin. In the tests, the leading-edge region of the lower portion of the vertical tail (where an air intake is located on the actual airplane) has been modified from a blunt nose to an elliptical nose.

External stores and other configuration modifications. - Various tanks and combinations of tanks were investigated on model configuration 3. Two sizes of wing-tip tanks were tested (fig. 7). The full-scale capacity of each of the small wing-tip tanks was 130 gallons, and that of each of the large wing-tip tanks was 230 gallons. One design of pylon-supported wing inboard tanks was tested and is shown in figure 8. Each of the wing inboard tanks had a full-scale capacity of 450 gallons. Four designs of pylon-supported center-line tanks were tested and are shown in figure 9. Center-line-tank configuration A had a full-scale capacity of 450 gallons; center-line-tank configurations B, C, and D each had a full-scale capacity of 650 gallons.

Various other model components were investigated on model configuration 3. Pylon-supported chaff dispensers and air-to-air missiles were tested and are indicated in figure 10. An afterbody bump (fig. 11) to provide additional capacity for fuel storage also improved the area distribution. Exit-nozzle blisters (fig. 12) were added to the end of the body for one test to reduce the severity of the slope of the area distribution at the end of the body.

The pylons used with the wing inboard tanks (fig. 8) and the chaff dispensers (fig. 10) were also tested without the stores, and they are designated herein as wing inboard pylons and wing outboard pylons, respectively.

Instrumentation

A six-component strain-gage balance, which was housed in the body, was used for determining the overall forces and moments on the model. A strain-gage attitude transmitter was used for getting the no-load angle of attack of the model. The attitude transmitter was housed in the extension of the model sting; thus, a correction to the reading of the attitude transmitter was necessary to obtain the model angle of attack because of flexibility under aerodynamic load of the balance, the model sting, and the sting extension.

Two static-pressure orifices were located within the chamber surrounding the strain-gage balance. These orifices were joined to a common tube and connected to a pressure transducer. Two other static-pressure orifices were located on the sides of the sting, adjacent to

the base of the body.  These orifices were also joined to a common tube and connected to a second pressure transducer.  A sting-mounted rake was used at the duct exit when mass-flow and internal-drag measurements were made.  The rake consisted of 2 static-pressure tubes and 12 total-pressure tubes (fig. 13).  A static-pressure tube was attached to the rim of the body base when duct exits B and C (fig. 3) were used (during the mass-flow measurements).

The overall forces and moments on the model, the angle of attack, and the static pressure in the chamber surrounding the strain-gage balance and at the sides of the sting at the body base were recorded electronically on punch cards.  During the mass-flow tests the pressures at the duct exit were measured by use of a multiple-tube manometer containing tetrabromoethane.  All manometer tubes were photographed simultaneously.

## TESTS, CORRECTIONS, AND ACCURACY

### Tests

Most of the tests were made with the model in the smooth condition. A few tests were made to determine the effect of fixed transition.  For such tests 0.1-inch-wide strips of No. 120 carborundum grains were shellacked on the upper and lower surfaces of the wing at 10 percent chord and on the body at 10 percent length.

All configurations were investigated through a range of angles of attack, and all configurations except those with the center-line tanks were tested at eight Mach numbers from 0.60 to 1.20.  The center-line-tank configurations were tested up to a Mach number of 0.99, inasmuch as these tanks are not intended to be carried at supersonic speeds.  The total pressure in the 8-foot transonic tunnel during the investigation was approximately 1 atmosphere, and the angle-of-attack range was approximately -2° to 17° at a Mach number of 0.60 and -2° to 9° at a Mach number of 1.20.  The maximum angles of attack were limited by balance loads.  In order to extend the angle-of-attack range, the tests in the 8-foot transonic pressure tunnel were made at a total pressure of 3/4 atmosphere; therefore, the corresponding angle-of-attack range was approximately -2° to 22° at a Mach number of 0.60 and -2° to 13° at a Mach number of 1.20.  One configuration was also tested in the 8-foot transonic pressure tunnel at a total pressure of 1 atmosphere.  The angle of sideslip was 0° for all tests.

The average Reynolds number of the investigation in the two tunnels is shown plotted against Mach number in figure 14.  The Reynolds number differences in the two tunnels at a total pressure of 1 atmosphere are

8

associated with the temperature differences in the two tunnels. The average stagnation temperature of the investigation in the 8-foot transonic tunnel varied from approximately $100^\circ$ F (at a Mach number of 0.60) to $175^\circ$ F (at a Mach number of 1.20). The stagnation temperature of the investigation in the 8-foot transonic pressure tunnel was $121^\circ$ F at all Mach numbers.

All the configurations were investigated with internal flow in the model. Duct exit A (fig. 3) was normally used. The static pressure in the chamber surrounding the strain-gage balance and at the sides of the sting at the body base was measured for all configurations. Except when mass-flow measurements were being made, the mass-flow rake was detached from the sting.

The mass flow and internal drag of model configuration 3 was determined for duct exits A, B, and C. The mass flow and internal drag were also determined for model configuration 3 with the exit-nozzle blisters, since the exit-nozzle blisters were found to affect the base pressures and thereby modify the mass flow. Duct exit A was used on the configuration with the exit-nozzle blisters. The bleeder ports were closed in all the mass-flow tests. Internal-flow data were obtained through the angle-of-attack range at Mach numbers from 0.60 to 1.20 for the configurations with duct exits A and B. Duct exit C was investigated only at angles of attack of $0^\circ$ and $4^\circ$ at Mach numbers from 0.60 to 0.99. The static pressure at the rim of the body base was measured when duct exits B and C were used. Strain-gage-balance data were also taken during the mass-flow tests.

## Corrections

The external-drag coefficient $C_D$ was corrected by adjusting the value of static pressure in the balance chamber and at the rim of the body base to the free-stream value. The external-drag coefficient also includes the correction for the internal-drag coefficient $C_{D,i}$. The internal-drag coefficient measured for model configuration 3 (duct exit A) was also used in correcting all the other configurations except the one with the exit-nozzle blisters. The internal-drag coefficient of the configuration with the exit-nozzle blisters was measured. A correction for buoyancy was made to the drag results at a Mach number of 1.20. This correction consisted of reducing the measured drag coefficients by 0.0018 in the investigation in the 8-foot transonic tunnel and by 0.0005 in the investigation in the 8-foot transonic pressure tunnel. No buoyancy correction was necessary at the other Mach numbers.

The lift and pitching-moment coefficients were not corrected for internal flow. The maximum correction to lift coefficient occurred at the highest angles of attack and amounted to only 0.005.

At subsonic Mach numbers, the interference effects of a tunnel boundary on the flow over a model in the test region near the center line of a tunnel have been made negligible by means of a slotted test section. Data are presented herein at supersonic Mach numbers of 1.03 and 1.20. Tunnel-boundary interference (tunnel-boundary-reflected compression and expansion disturbances) on the data at a Mach number of 1.03 was probably small and is believed to have been confined primarily to affecting the drag data. The data at a Mach number of 1.20 are considered free of tunnel-boundary interference. No corrections have been made to the data at a Mach number of 1.03 for tunnel-boundary interference except to the extent of the partial correction for tunnel-boundary interference inherent in the base-pressure correction.

No sting-interference corrections have been made to the data except to the extent of the partial correction for sting interference inherent in the base-pressure correction.

## Accuracy

The accuracy of the data, based primarily on the static calibrations and the repeatability of the data, is estimated to be as follows:

$C_L$ . . . . . . . . . . . . . . . . . . . . . . . . . . . . . . . . ±0.01
$C_D$ . . . . . . . . . . . . . . . . . . . . . . . . . . . . . . . . ±0.001
$C_m$ . . . . . . . . . . . . . . . . . . . . . . . . . . . . . . . ±0.003
$\alpha$, deg . . . . . . . . . . . . . . . . . . . . . . . . . . . . . ±0.1
M . . . . . . . . . . . . . . . . . . . . . . . . . . . . . . . . . ±0.003

## PRESENTATION OF RESULTS

The basic longitudinal aerodynamic characteristics for the various configurations are presented in figures 15 to 27. All configurations were tested at a horizontal-tail deflection of -3° and at an angle of sideslip of 0°. These basic results are presented as follows:

Summary data on performance and longitudinal-stability derivatives are shown in figures 28 to 38. Figure 38 includes results at Mach numbers of 1.57 and 2.01 from reference 1. Internal-drag coefficient and mass-flow ratio are plotted against angle of attack, Mach number, and duct exit area in figure 39. The derivatives $C_{L_\alpha}$ and $C_{m_{C_L}}$ shown herein are for a lift coefficient of approximately zero. The drag-rise factor $\Delta C_D/\Delta C_L^2$ shown herein is an average value applicable up to a lift coefficient of approximately 0.5. These summary figures are presented as follows:

## DISCUSSION

### Effects of Test Conditions

An increase in the total pressure (and Reynolds number) in the 8-foot transonic pressure tunnel from 3/4 atmosphere to 1 atmosphere

had negligible effect on the longitudinal aerodynamic characteristics of model configuration 3 (figs. 15(a) and 28(a)). The Reynolds numbers corresponding to these two values of total pressure are shown in figure 14.

The lift, drag, and pitching-moment results obtained in the two tunnels on the same configurations were generally in good agreement (figs. 15 and 28). The greatest differences were observed in drag coefficient at a Mach number of 1.03 and in pitching-moment coefficient at high angles of attack at a Mach number of 0.99. These differences occurred at Mach numbers where the coefficients were changing rapidly with Mach number, so that small errors in Mach number can result in seemingly large errors in the coefficients. The drag results at a Mach number of 1.03 were also probably affected differently by the wall-reflected disturbances in the two tunnels. (See section entitled "Apparatus" for a discussion of the differences in the test sections of the two tunnels.) The tests of model configuration 3 in the 8-foot transonic pressure tunnel at total pressures of 3/4 atmosphere and 1 atmosphere indicate that the Reynolds number differences in the two tunnels had no significant effect on the longitudinal aerodynamic characteristics.

Fixing transition on the model had negligible effect on the lift and pitching-moment characteristics and resulted in the usual increases in drag coefficient (figs. 16 and 29).

## Longitudinal Stability

The variation of pitching-moment coefficient with lift coefficient was stable, although generally nonlinear, for all configurations investigated at all test Mach numbers. No serious pitch-up difficulties were apparent at a constant Mach number, although some minor decreases in longitudinal stability were evident at several Mach numbers. The greatest effect of configuration modifications on pitching-moment characteristics was a change in trim equivalent to about $2^\circ$ of horizontal-tail deflection (based on unpublished horizontal-tail-effectiveness results) and a change in stability corresponding to a movement of the aerodynamic center of about 5 percent of the mean aerodynamic chord. The largest trim change occurred when the wing inboard tanks and the chaff dispensers (fig. 22) or the exit-nozzle blisters (fig. 25) were installed. The maximum change in longitudinal stability occurred when the large wing-tip tanks were installed (fig. 32). In general, the longitudinal stability was not adversely affected by configuration modifications.

### Effects of Configuration Modifications

During the investigation it was found that the large and the small two-place canopies showed no differences in the longitudinal aerodynamic characteristics except for a somewhat higher drag coefficient for the large canopy (figs. 18(c) and 30(c)). Accordingly, no further tests of the small two-place canopy were made. Replacement of the single-place canopy by the large two-place canopy caused a small increase in drag coefficient at most test Mach numbers and in lift-curve slope at Mach numbers near 1 (figs. 18 and 30). The longitudinal stability was unaffected by this change to the large two-place canopy, although a small shift in trim to higher lift coefficients occurred.

The longer body nose had no significant effect on longitudinal aerodynamic characteristics (figs. 18 and 30).

The biggest effect of configuration modifications on lift occurred when the wing-tip tanks were installed. The small wing-tip tanks increased the lift-curve slope by 7 or 8 percent over the Mach number range, and the large wing-tip tanks increased the lift-curve slope by about 11 percent (fig. 32).

The afterbody bump (for fuel storage) and the exit-nozzle blisters each reduced the drag coefficient at zero lift by about 0.002 at sonic and supersonic speeds (fig. 36). This reduction in drag can be attributed to the improvement in area distribution resulting from the addition of the bump and the blisters.

External stores caused substantial increases in drag. Model configuration 3 with the center-line-tank configurations A, B, C, and D showed no significantly different longitudinal aerodynamic characteristics other than a somewhat lower drag for the model with the smaller tank A (figs. 20 and 31). The incremental drag coefficient at zero lift of the larger center-line-tank configurations was about 0.010 at a Mach number of 0.99. At a Mach number of 1.20 the incremental drag coefficient at zero lift of the wing inboard tanks was about 0.010 and that of the combination of wing inboard tanks and chaff dispensers was about 0.022 (fig. 33). The two sizes of wing-tip tanks produced essentially the same drag (figs. 21 and 32). The incremental drag coefficient at zero lift of the wing-tip tanks was about 0.005 at a Mach number of 1.2 (fig. 32).

### Mach Number Effects

Figure 38 shows the variation with Mach number of the performance and longitudinal-stability derivatives of model configurations 1 and 3 for Mach numbers from 0.60 to 2.01. The subsonic and transonic results

are from figure 30(a). The results at Mach numbers of 1.57 and 2.01 are from reference 1. Model configuration 1 had the small body nose and the single-place canopy, and model configuration 3 had the long body nose and the large two-place canopy. It is seen that the longitudinal aero-dynamic characteristics of these two configurations were essentially the same except for quite small differences in drag - the drag coefficient of model configuration 3 was higher than that of model configuration 1, at most by 0.002 at supersonic speeds. The rearward movement of the aerodynamic center at transonic and supersonic speeds amounted to about 27 percent of the mean aerodynamic chord. A small forward movement of the aerodynamic center was evident at Mach numbers from 1.57 to 2.01. The lift-curve slope at a Mach number of 2.01 was about three-fourths of its value at a Mach number of 0.60, and the maximum lift-drag ratio at a Mach number of 2.01 was about one-half of its low-speed value.

## Internal Flow

The mass-flow survey rake had negligible effect on longitudinal aerodynamic characteristics other than a small decrease in drag coef-ficient (fig. 26). This drag reduction was probably due to the influence of the pressure field of the rake on the rearward portion of the model. A reduction in the duct exit area reduced the mass flow and the internal drag (fig. 39(c)) and had slight effect on lift and pitching moment (figs. 27 and 37). The maximum reduction in duct exit area (45 percent) increased the drag coefficient (figs. 27 and 37); the increase amounted to about 0.0035 at zero lift. This increase in external drag generally would be expected because of the additional spillage of air from the inlet. The intermediate reduction in duct exit area (26 percent) increased the drag somewhat at a Mach number of 1.20 and, at the higher lift coefficients, at test Mach numbers lower than 1.20 (fig. 27).

Opening the inlet-duct bleeder ports had no important effect on the longitudinal aerodynamic characteristics as shown by figure 17.

## CONCLUDING REMARKS

An investigation was made in the Langley 8-foot transonic tunnel and the Langley 8-foot transonic pressure tunnel of the static longi-tudinal stability and performance characteristics of various configura-tions of a 1/22-scale model of a supersonic fighter-bomber airplane. The Mach number range of the tests was generally from 0.60 to 1.20. All the configurations were investigated with internal flow in the model. Configurations included single-place and two-place canopies, short and long body noses, external stores, an afterbody bump for fuel storage, and exit-nozzle blisters.

The effect of configuration modifications on longitudinal stability and trim was small. Area-rule modifications showed some drag reductions at sonic and supersonic speeds. External stores caused substantial increases in drag.

Langley Research Center,
    National Aeronautics and Space Administration,
        Langley Field, Va., January 17, 1961.

# REFERENCES

1. Appich, W. H., Jr., Oehman, Waldo I., and Gregory, Donald T.: Aero-dynamic Characteristics of Three Versions of a Supersonic Airplane Model With a 45° Sweptback Midwing at Mach Numbers of 1.57 and 2.01. NASA MEMO 12-6-58L, 1959.

2. Wright, Ray H., Ritchie, Virgil S., and Pearson, Albin O.: Charac-teristics of the Langley 8-Foot Transonic Tunnel With Slotted Test Section. NACA Rep. 1389, 1958. (Supersedes NACA RM L51H10 by Wright and Ritchie and RM L51K14 by Ritchie and Pearson.)

3. Platt, Robert J., Jr., and Brooks, Joseph D.: Transonic Wind-Tunnel Investigation of the Effects of Sweepback and Thickness Ratio on the Wing Loads of a Wing-Body Combination of Aspect Ratio 4 and Taper Ratio 0.6. NACA RM L54L31b, 1955.

TABLE I.- GEOMETRIC CHARACTERISTICS OF MODEL CONFIGURATIONS
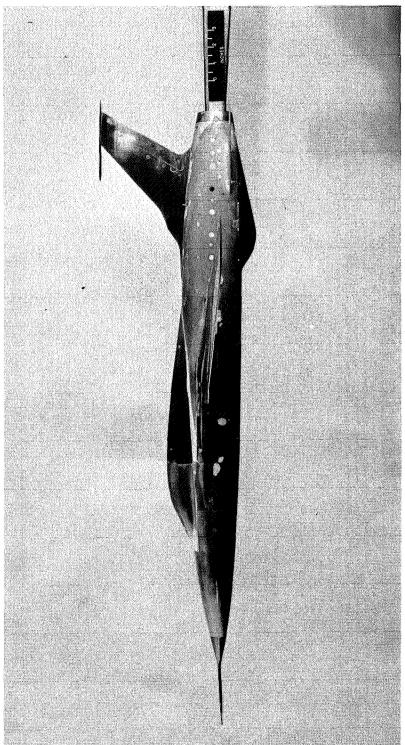
Body:
  Length -
    With short nose, in. . . . . . . . . . . . . . . . . . . . . . . . . . . . . . . . . . . . . . . . . . 33.742
    With long nose, in. . . . . . . . . . . . . . . . . . . . . . . . . . . . . . . . . . . . . . . . . . . 35.318
  Maximum width, in. . . . . . . . . . . . . . . . . . . . . . . . . . . . . . . . . . . . . . . . . . . . 2.92
  Maximum depth (excluding canopy), in. . . . . . . . . . . . . . . . . . . . . . . . . . . . . . . . . . 3.73
  Frontal area (including large two-place canopy), sq ft . . . . . . . . . . . . . . . . . . . . . . . . . 0.060
  Side area (including large two-place canopy) -
    With short nose, sq ft . . . . . . . . . . . . . . . . . . . . . . . . . . . . . . . . . . . . . . . 0.780
    With long nose, sq ft . . . . . . . . . . . . . . . . . . . . . . . . . . . . . . . . . . . . . . . . 0.805
  Frontal area/Wing area . . . . . . . . . . . . . . . . . . . . . . . . . . . . . . . . . . . . . . . . 0.076
  Total base area (includes duct exit area)/Wing area . . . . . . . . . . . . . . . . . . . . . . . . . 0.0307

Wing:
  Airfoil section (parallel to body reference line) -
    At 0.38-semispan station . . . . . . . . . . . . . . . . . . . . . . . . . . . . . . . . NACA 65A005.5
    Tip . . . . . . . . . . . . . . . . . . . . . . . . . . . . . . . . . . . . . . . . . . . NACA 65A003.7
  Root chord, $c_r$ -
    Length, in. . . . . . . . . . . . . . . . . . . . . . . . . . . . . . . . . . . . . . . . . . . . 8.181
    Incidence with respect to body reference line, deg . . . . . . . . . . . . . . . . . . . . . . . . 0
    Location above body reference line, in. . . . . . . . . . . . . . . . . . . . . . . . . . . . . . 0.614
    Location (parallel to body reference line) of leading edge of root chord from nose (long) of body, in. . . . 14.243
  Tip chord, $c_t$, in. . . . . . . . . . . . . . . . . . . . . . . . . . . . . . . . . . . . . . . . . 3.818
  Span, b, in. . . . . . . . . . . . . . . . . . . . . . . . . . . . . . . . . . . . . . . . . . . . . 19.054
  Area, S, sq ft . . . . . . . . . . . . . . . . . . . . . . . . . . . . . . . . . . . . . . . . . . . 0.794
  Aspect ratio, A . . . . . . . . . . . . . . . . . . . . . . . . . . . . . . . . . . . . . . . . . . . 3.18
  Taper ratio, $\lambda$ . . . . . . . . . . . . . . . . . . . . . . . . . . . . . . . . . . . . . . . 0.467
  Mean aerodynamic chord -
    Length, in. . . . . . . . . . . . . . . . . . . . . . . . . . . . . . . . . . . . . . . . . . . . 6.264
    Location above body reference line, in. . . . . . . . . . . . . . . . . . . . . . . . . . . . . . 0.358
    Location (parallel to body reference line) of leading edge of mean aerodynamic chord from
      leading edge of root chord, in. . . . . . . . . . . . . . . . . . . . . . . . . . . . . . . . 4.666
  Sweepback of projected 25-percent-chord line, deg . . . . . . . . . . . . . . . . . . . . . . . . . . 45
  Dihedral, deg . . . . . . . . . . . . . . . . . . . . . . . . . . . . . . . . . . . . . . . . . . . . -3.5
  Twist, deg . . . . . . . . . . . . . . . . . . . . . . . . . . . . . . . . . . . . . . . . . . . . . 0

Horizontal tail:
  Type . . . . . . . . . . . . . . . . . . . . . . . . . . . . . . . . . . . . . . . . . . . . . All movable
  Airfoil section (parallel to model plane of symmetry) -
    Root . . . . . . . . . . . . . . . . . . . . . . . . . . . . . . . . . . . . . . . . . . . NACA 65A006
    96-percent-semispan station . . . . . . . . . . . . . . . . . . . . . . . . . . . . . . . NACA 65A004
  Root chord, in. . . . . . . . . . . . . . . . . . . . . . . . . . . . . . . . . . . . . . . . . . . 4.091
  Tip chord, in. . . . . . . . . . . . . . . . . . . . . . . . . . . . . . . . . . . . . . . . . . . . 1.767
  Span, in. . . . . . . . . . . . . . . . . . . . . . . . . . . . . . . . . . . . . . . . . . . . . . 9.488
  Area (total), sq ft . . . . . . . . . . . . . . . . . . . . . . . . . . . . . . . . . . . . . . . . 0.193
  Aspect ratio . . . . . . . . . . . . . . . . . . . . . . . . . . . . . . . . . . . . . . . . . . . . 3.24
  Taper ratio . . . . . . . . . . . . . . . . . . . . . . . . . . . . . . . . . . . . . . . . . . . . 0.432
  Mean aerodynamic chord -
    Length, in. . . . . . . . . . . . . . . . . . . . . . . . . . . . . . . . . . . . . . . . . . . . 3.083
    Location of leading edge of mean aerodynamic chord from leading edge of root chord, in. . . . . . . . . 2.310
  Sweepback of 25-percent-chord line, deg . . . . . . . . . . . . . . . . . . . . . . . . . . . . . . . 45
  Dihedral, deg . . . . . . . . . . . . . . . . . . . . . . . . . . . . . . . . . . . . . . . . . . . . 0
  Twist, deg . . . . . . . . . . . . . . . . . . . . . . . . . . . . . . . . . . . . . . . . . . . . . 0

Vertical tail:
  Airfoil section (parallel to body reference line) -
    Root . . . . . . . . . . . . . . . . . . . . . . . . . . . . . . . . . . . . . . . . . . . NACA 65A006
    Tip . . . . . . . . . . . . . . . . . . . . . . . . . . . . . . . . . . . . . . . . . . . NACA 65A004
  Root chord (at body reference line), in. . . . . . . . . . . . . . . . . . . . . . . . . . . . . . . 5.903
  Tip chord, in. . . . . . . . . . . . . . . . . . . . . . . . . . . . . . . . . . . . . . . . . . . . 2.000
  Span (to body reference line), in. . . . . . . . . . . . . . . . . . . . . . . . . . . . . . . . . . 7.136
  Area (to body reference line), sq ft . . . . . . . . . . . . . . . . . . . . . . . . . . . . . . . . 0.196
  Aspect ratio $\left(\dfrac{(\text{Span})^2}{\text{Area}}\right)$ . . . . . . . . . . . . . . . . . . . . . . . . . . . . . 1.81
  Taper ratio . . . . . . . . . . . . . . . . . . . . . . . . . . . . . . . . . . . . . . . . . . . . 0.339
  Mean aerodynamic chord -
    Length, in. . . . . . . . . . . . . . . . . . . . . . . . . . . . . . . . . . . . . . . . . . . . 4.273
    Location (parallel to body reference line) of leading edge of mean aerodynamic chord from
      leading edge of root chord, in. . . . . . . . . . . . . . . . . . . . . . . . . . . . . . . . 3.307
    Location (spanwise) of mean aerodynamic chord from root chord, in. . . . . . . . . . . . . . . . . 2.981
  Sweepback of leading edge, deg . . . . . . . . . . . . . . . . . . . . . . . . . . . . . . . . . . . 48.0

Duct areas:
  Supersonic inlet (cruise condition) -
    Inlet throat (scaled down from full-scale), sq in. . . . . . . . . . . . . . . . . . . . . . . . . 1.612
    Projected inlet (scaled down from full-scale), sq in. . . . . . . . . . . . . . . . . . . . . . . . 1.787
  Exit (see fig. 3) -
    Duct exit A, sq in. . . . . . . . . . . . . . . . . . . . . . . . . . . . . . . . . . . . . . . . 2.024
    Duct exit B, sq in. . . . . . . . . . . . . . . . . . . . . . . . . . . . . . . . . . . . . . . . 1.507
    Duct exit C, sq in. . . . . . . . . . . . . . . . . . . . . . . . . . . . . . . . . . . . . . . . 1.109

Figure 1.- General arrangement of model configuration 3. All dimensions are in inches except as noted.

Mean aerodynamic chord

25-percent-chord line

Horizontal-tail hinge line

1.767

45°

3.292

3.818

4.186 4.091

16.264

45°

8.181

.25-percent-chord line

28.748

20.476

14.243

Sting

7.136

2.000

Antenna tip

9.917

48°

5.903

c.g. location at 0.25 c̄

35.38

25.657

20.476

19.794

Body reference line

Body station 0

.509

3.5°

.818

9.488

19.054

.358
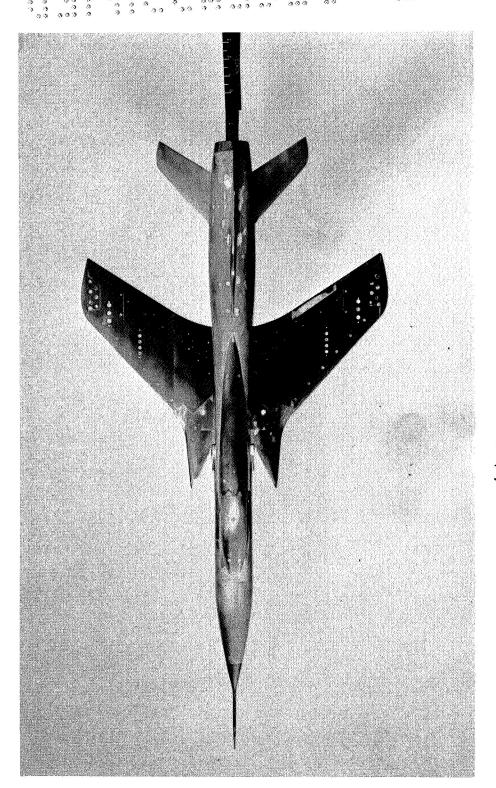
(a) Side view.

Figure 2.- Photographs of model configuration 3. $\delta_h = -3°$. L-58-2330
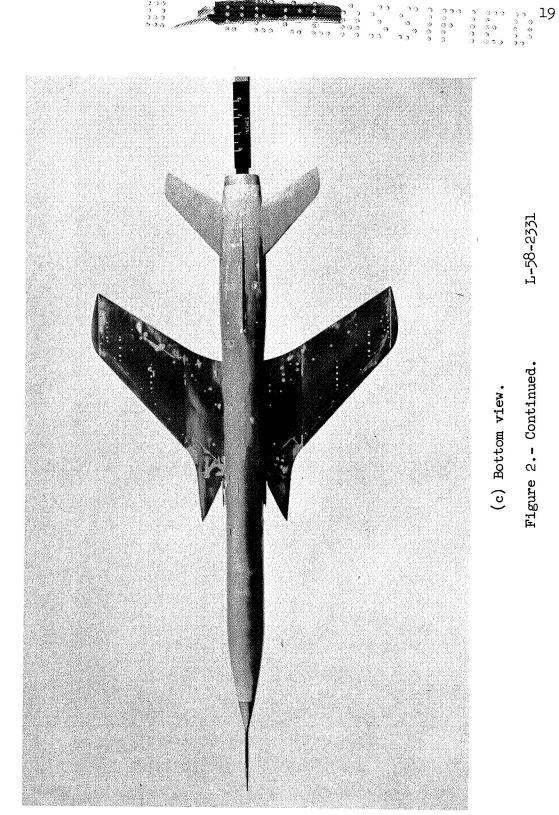
(b) Planform view.

Figure 2.- Continued.

L-58-2332

(c) Bottom view.

Figure 2.- Continued.

L-58-2331

(d) Closeup of left inlet showing boundary-layer diverter.    L-58-2333

Figure 2.- Concluded.
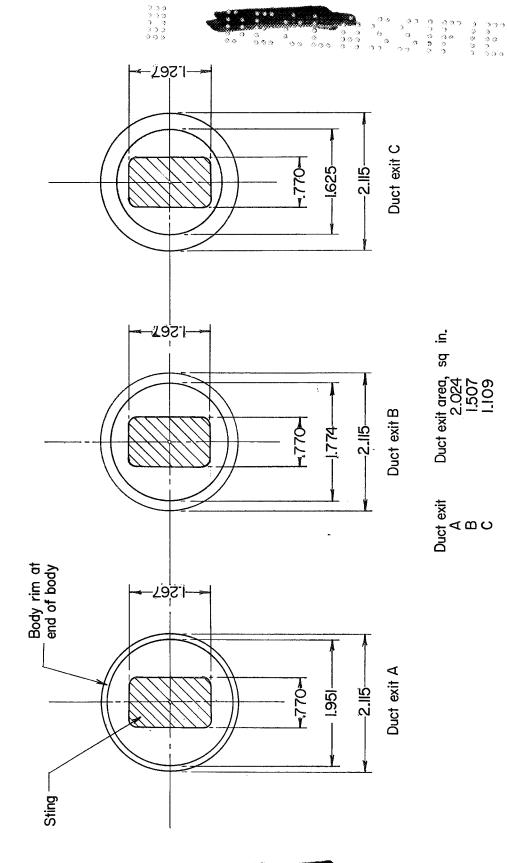
Figure 3.- Duct exits tested with supersonic inlet (cruise condition) and sting cross section at end of body. All dimensions are in inches except as noted.

| Duct exit | Duct exit area, sq in. |
|-----------|------------------------|
| A | 2.024 |
| B | 1.507 |
| C | 1.109 |

Duct exit A

Duct exit B

Duct exit C

Body rim at end of body

Sting

1.267

1.267

1.267

.770

.770

.770

1.951

1.774

1.625

2.115

2.115

2.115

Section showing bleeder port closed

.418

.209

.591

.295

A

A

Body station 22.000

Body reference line

Wing

Section A-A
(bleeder ports half open)
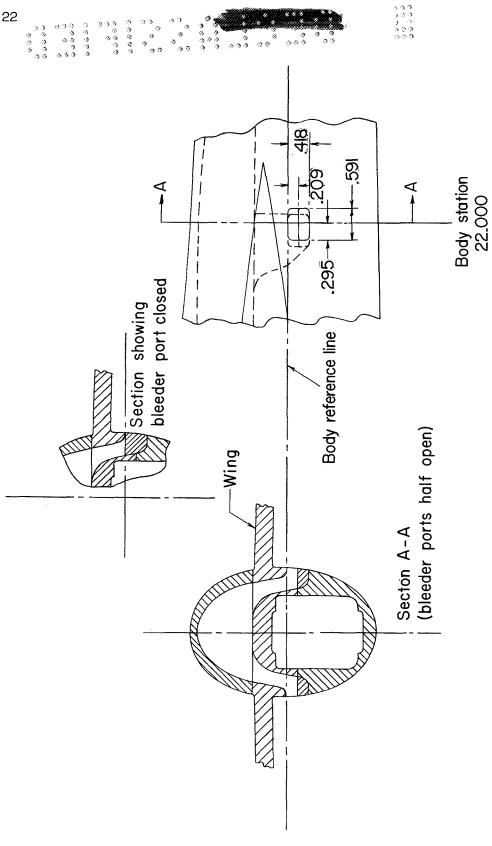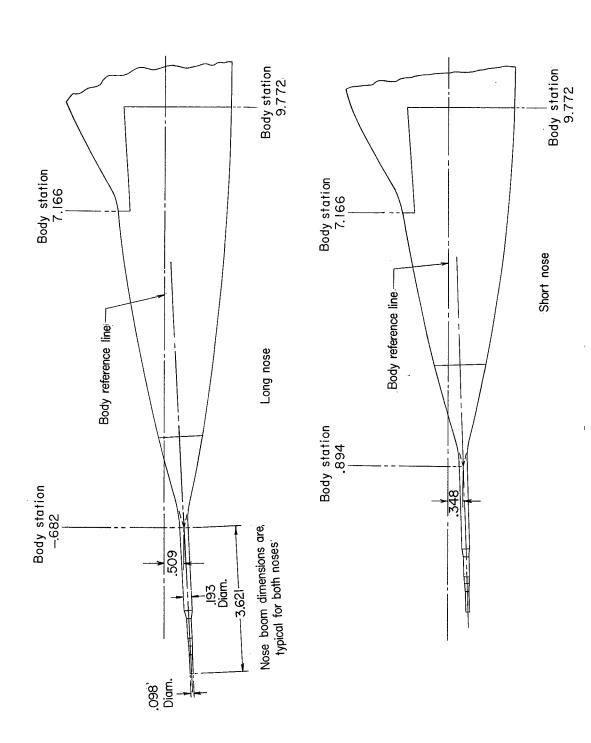
Figure 4.- Inlet-duct bleeder ports tested. All dimensions are in inches.

L-855

Body station
7.166

Body station
9.772

Body reference line

Long nose

Body station
-.682

.509

.193
Diam.

3.621

.098
Diam.

Nose boom dimensions are,
typical for both noses

Body station
7.166

Body station
9.772

Body reference line

Short nose

Body station
.894

.348

Figure 5.- Body noses tested. All dimensions are in inches.

Body station
12.726

Large two-place canopy
Small two-place canopy
Single-place canopy

A

A

Body reference line

Body station
7.166

Large two-place canopy
Small two-place canopy
Single-place canopy

Section A-A
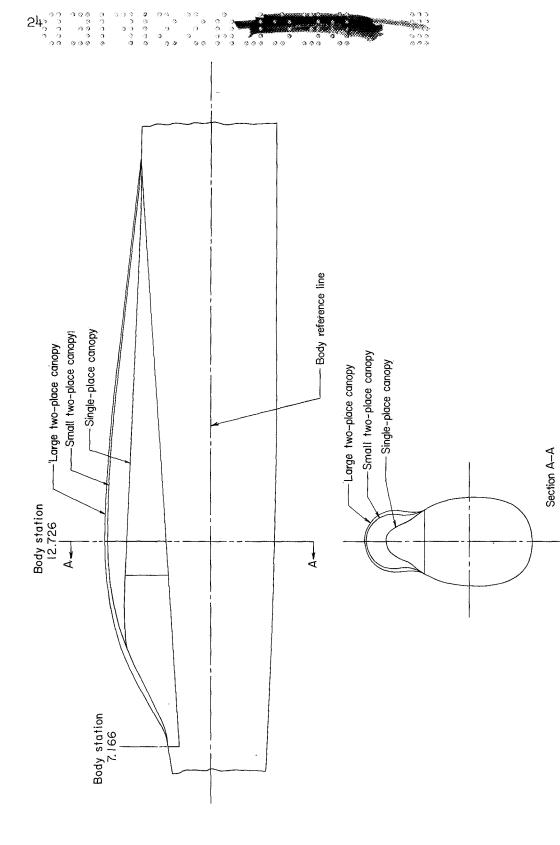
Figure 6.- Canopies tested. All dimensions are in inches.

Large tank

Small tank

.500

11.954

5.977

.500

9.882

4.941

.996
Diam.
(max.)

.824
Diam.
(max.)
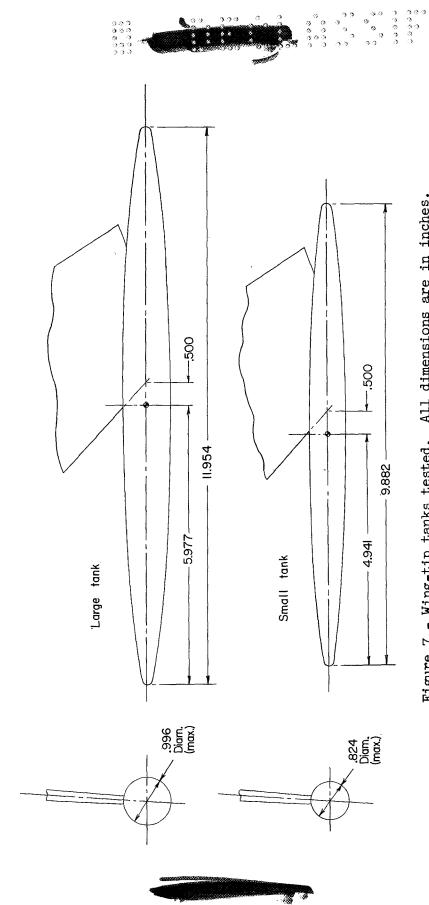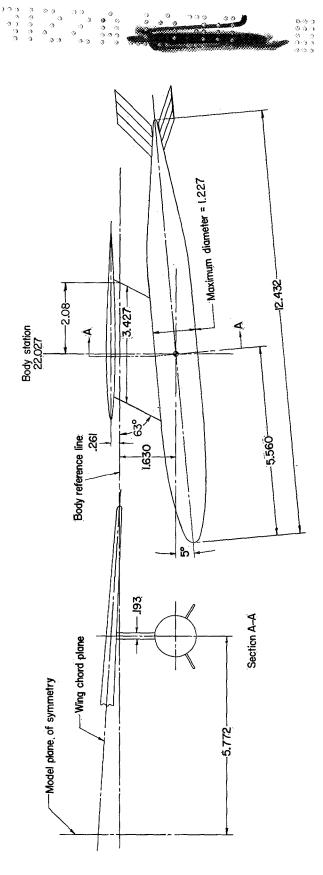
Figure 7.- Wing-tip tanks tested.  All dimensions are in inches.

Figure 8.- Wing inboard tanks tested. All dimensions are in inches except as noted.

View B-B
showing tank fins

Ventral fins

Maximum diameter = 1.227

11.715

Canopy

4.318

1.977

B

B

Body station
16.886

A

A

4.928

5°

Body reference line.

2.915

.097

15°

Section A-A
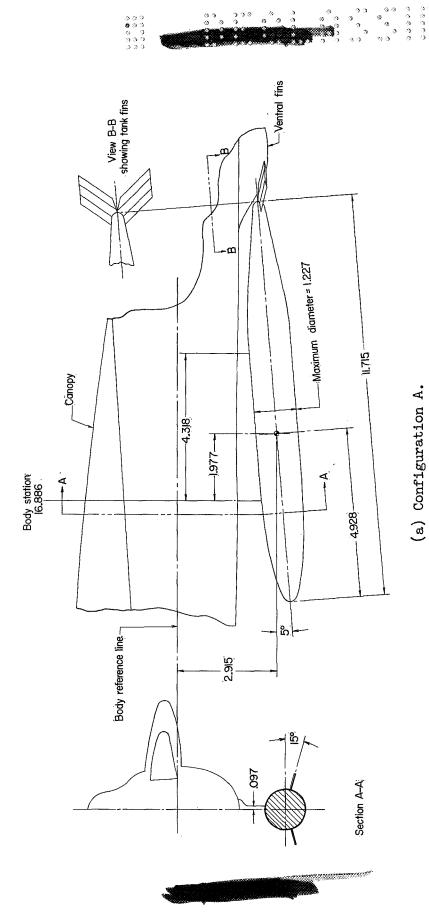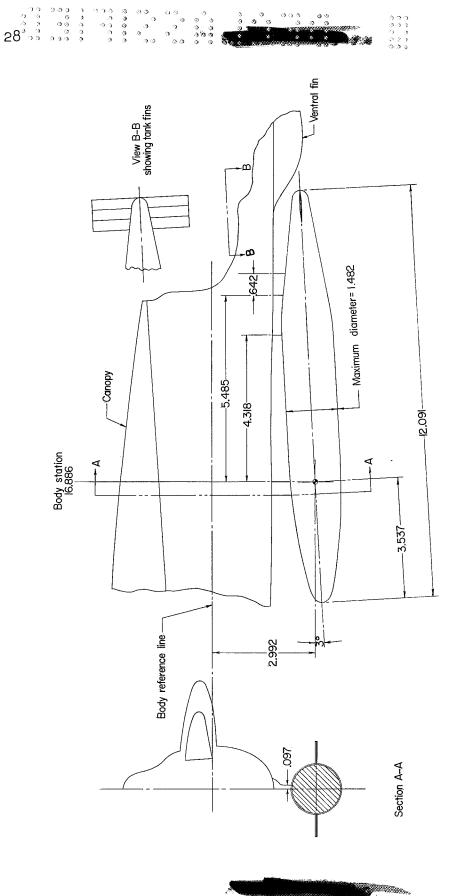
(a) Configuration A.

Figure 9.- Center-line tanks tested.  All dimensions are in inches except as noted.

View B-B
showing tank fins

Ventral fin

Canopy

Body station
16.886

.642

5.485

4.318

Maximum diameter=1.482

12.091

3.537

Body reference line

2.992

3°

.097

Section A-A
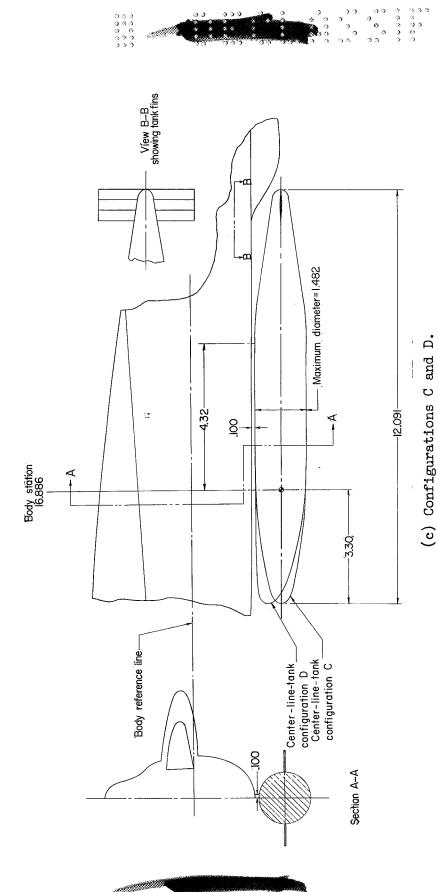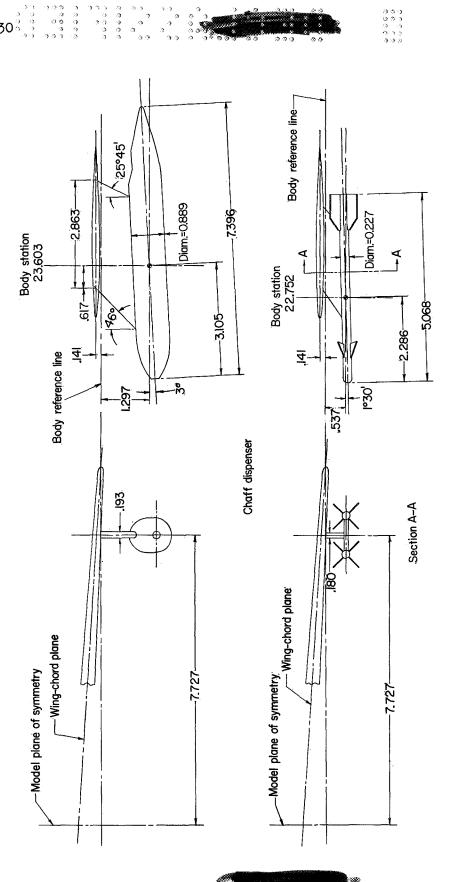
(b) Configuration B.

Figure 9.- Continued.

L-855

29

View B–B
showing tank fins

Maximum diameter=1.482

Body station
16.886

4.32

.100

12.091

3.30

Body reference line

Center-line-tank
configuration D
Center-line-tank
configuration C

.100

Section A–A

(c) Configurations C and D.

Figure 9.- Concluded.

Figure 10.- Chaff dispensers and air-to-air missiles tested. All dimensions are in inches except as noted.

L-855
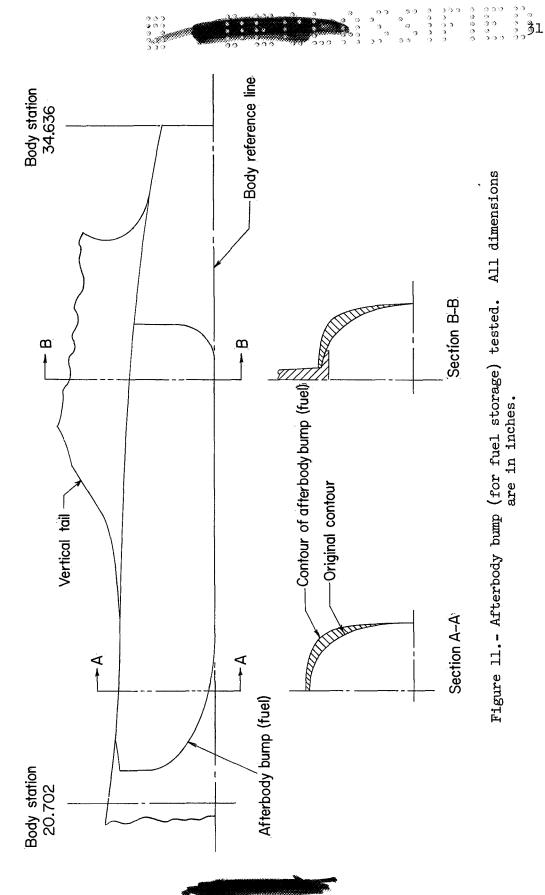
Figure 11.- Afterbody bump (for fuel storage) tested. All dimensions are in inches.

Section A-A

Body reference line

7.130

2.730

A

A

Body reference line
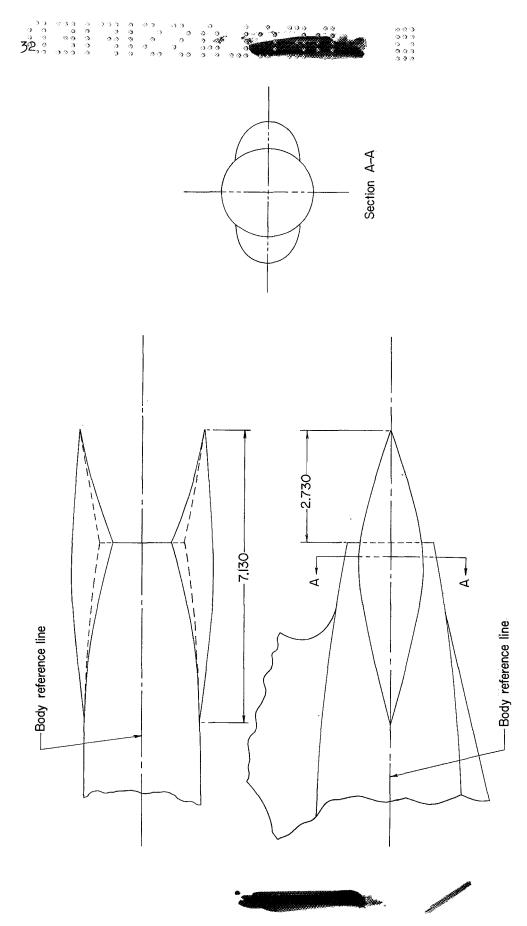
Figure 12.- Exit-nozzle blisters tested. All dimensions are in inches.
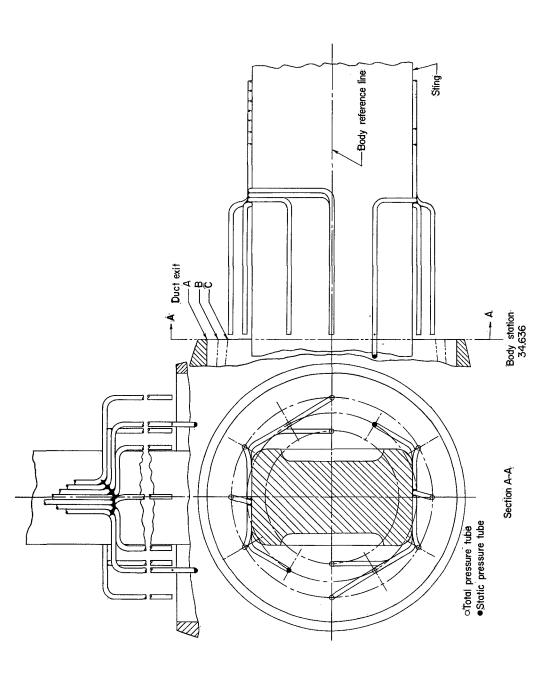
Figure 13.- Survey rake consisting of total-pressure and static-pressure tubes used in determining internal drag. All dimensions are in inches except as noted.
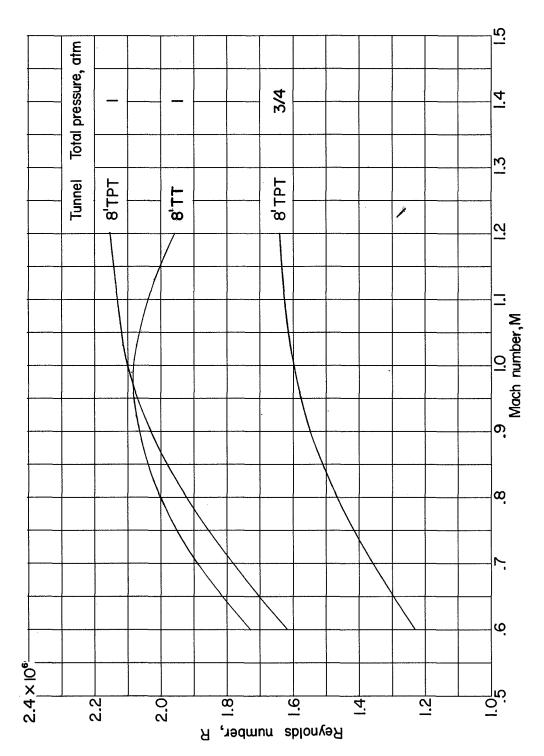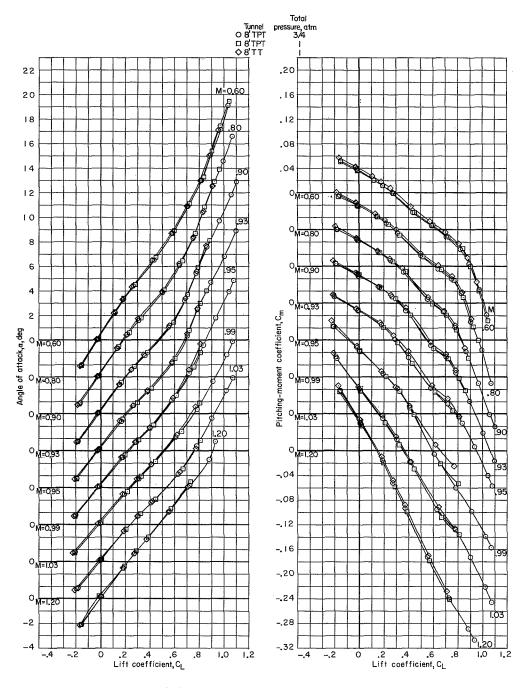
Figure 14.- Variation of average Reynolds number (based on wing mean aerodynamic chord of 6.264 inches) with Mach number in tests in Langley 8-foot transonic pressure tunnel (8' TPT) and the Langley 8-foot transonic tunnel (8' TT).
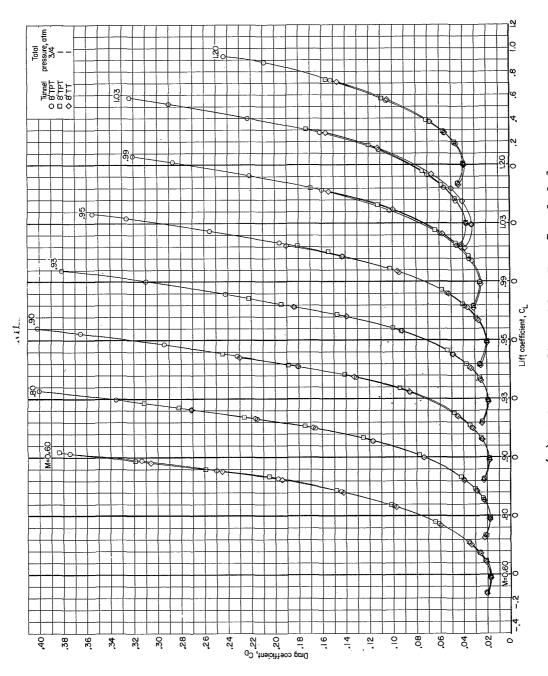
(a) Model configuration 3.

Figure 15.- Comparison of longitudinal aerodynamic characteristics of several configurations tested in both the 8' TPT and the 8' TT. $\delta_h = -3°$.
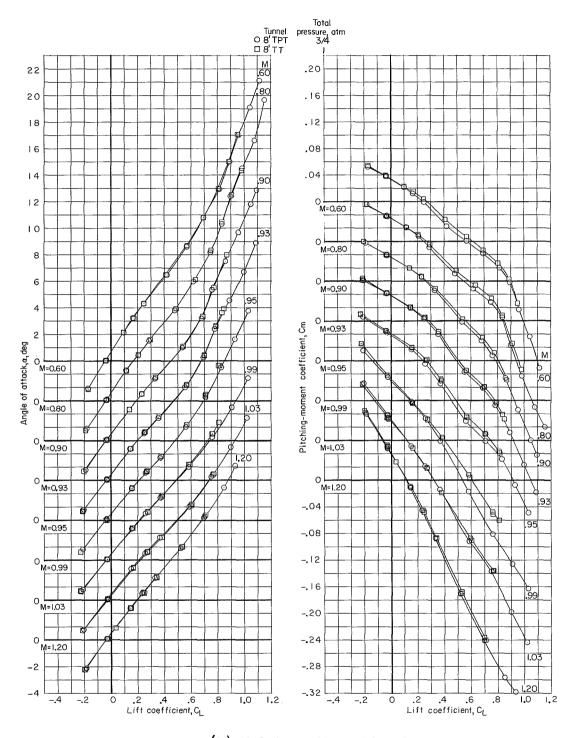
(a) Model configuration 3. Concluded.

Figure 15.- Continued.
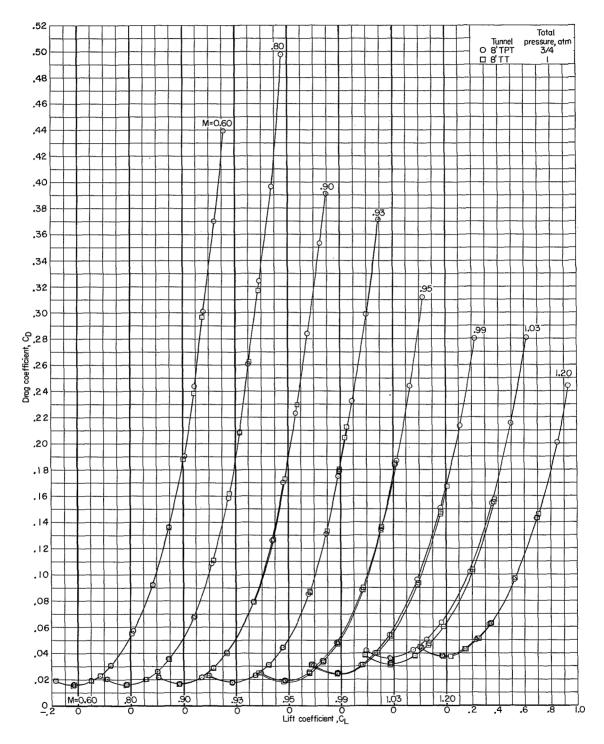
(b) Model configuration 1.

Figure 15.- Continued.
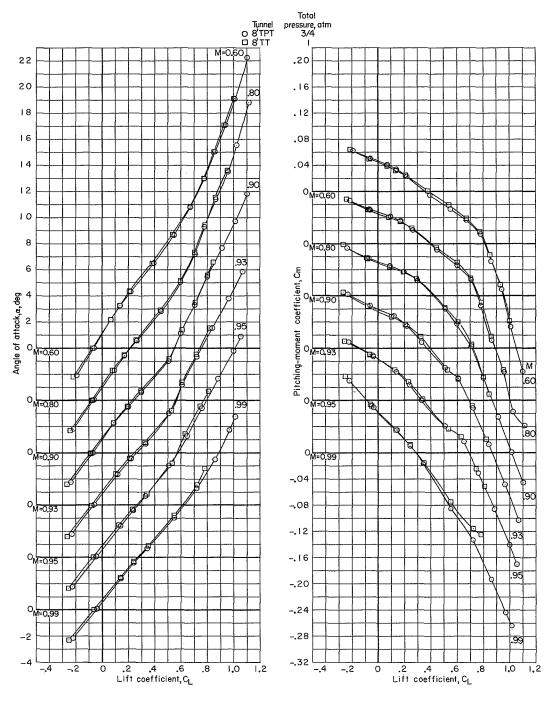
(b) Model configuration 1.  Concluded.

Figure 15.- Continued.
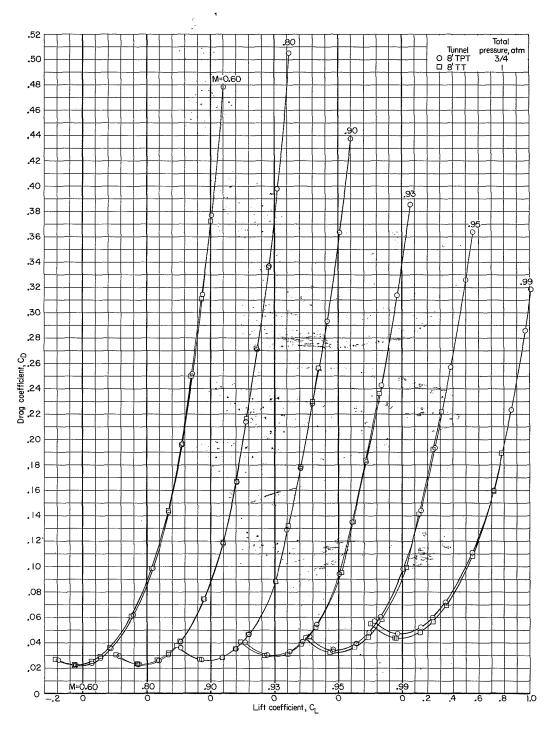
L-855



(c) Model configuration 3 plus wing inboard tanks and center-line-tank configuration B.

Figure 15.- Continued.
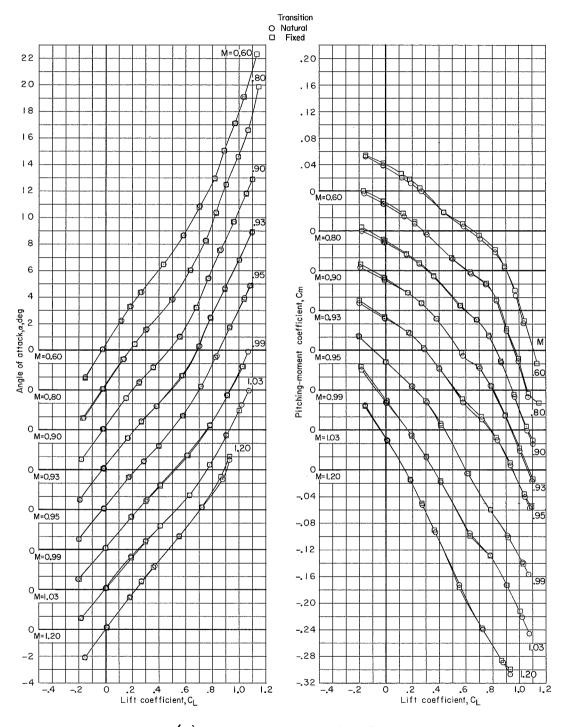
.52

.50

.48  M=0.60

.80

.46

.44  .90

.42

.40

.38  .93

.36  .95

.34

.32  .99

.30

.28

Drag coefficient, $C_D$

.26

.24

.22

.20

.18

.16

.14

.12

.10

.08

.06

.04

.02

0

M=0.60   .80   .90   .93   .95   .99

-.2   0   0   0   0   0   0   .2   .4   .6   .8   1.0

Lift coefficient, $C_L$

|  | Tunnel | Total pressure, atm |
|---|---|---|
| O | 8' TPT | 3/4 |
| □ | 8' TT | 1 |

(c) Model configuration 3 plus wing inboard tanks and center-line-tank configuration B.   Concluded.

Figure 15.- Concluded.
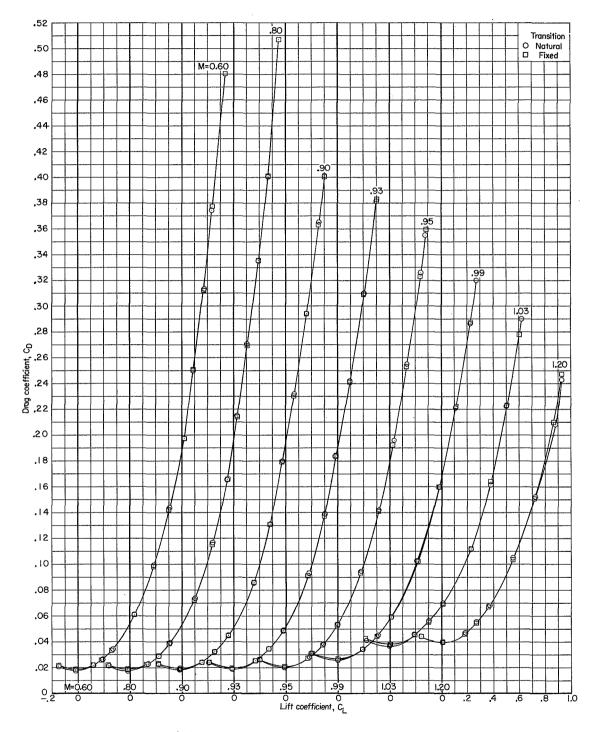
(a) Model configuration 3.

Figure 16.- Effect of fixed transition on longitudinal aerodynamic characteristics of several configurations. $\delta_h = -3^\circ$; 8' TPT.

L-855

(a) Model configuration 3.   Concluded.

Figure 16.- Continued.

L-855

Transition
○  Natural
□  Fixed
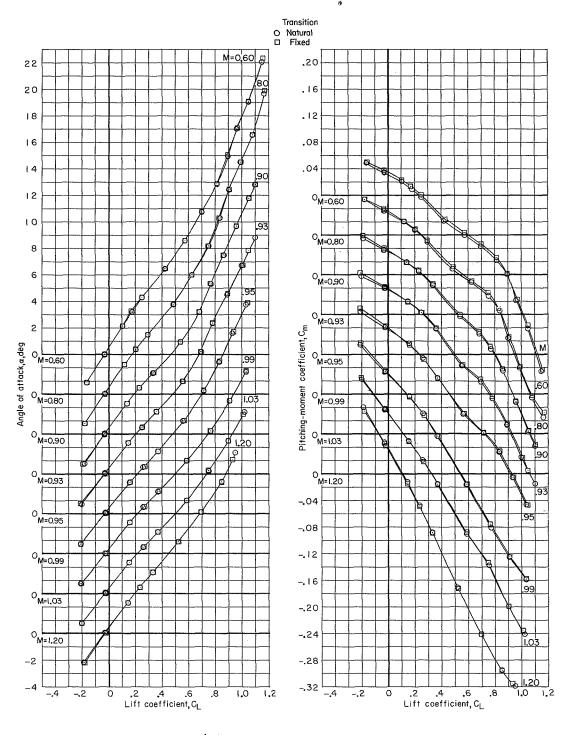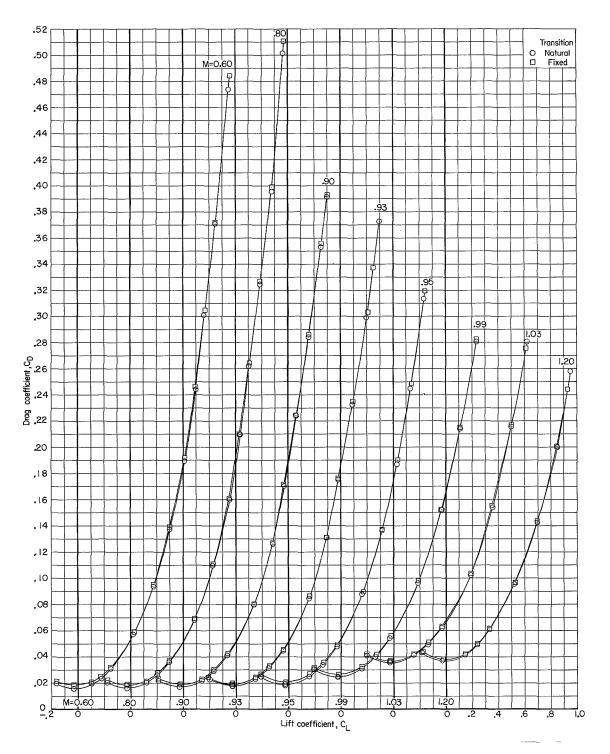


(b) Model configuration 5.

Figure 16.- Continued.
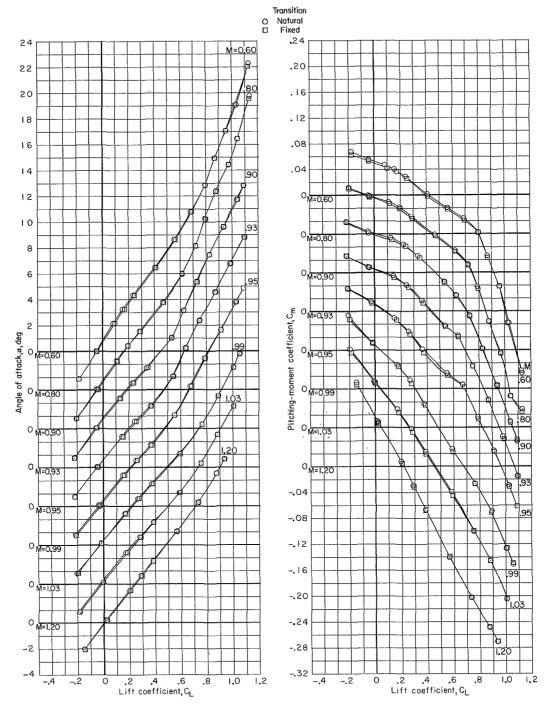
(b) Model configuration 5.  Concluded.

Figure 16.- Continued.

L-855
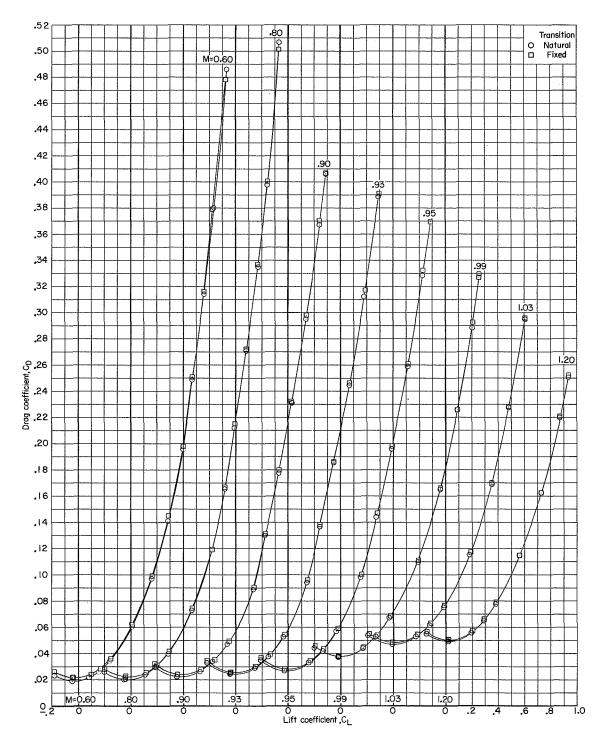


(c) Model configuration 3 plus wing inboard tanks.

Figure 16.- Continued.
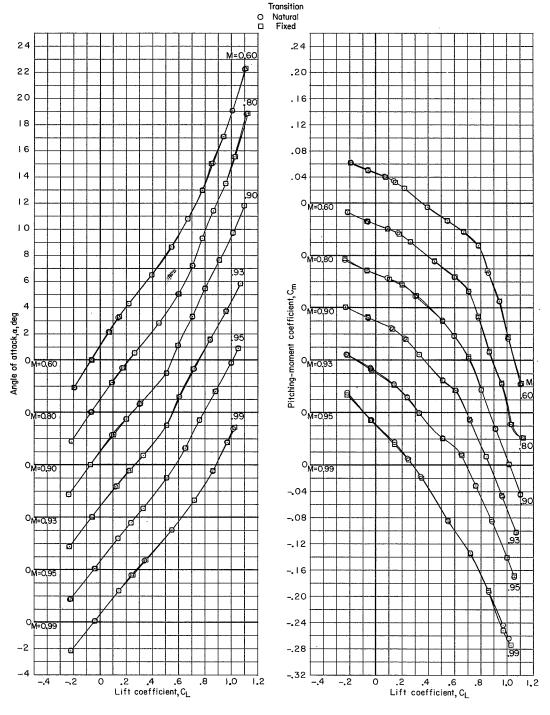
(c) Model configuration 3 plus wing inboard tanks.  Concluded.

Figure 16.- Continued.
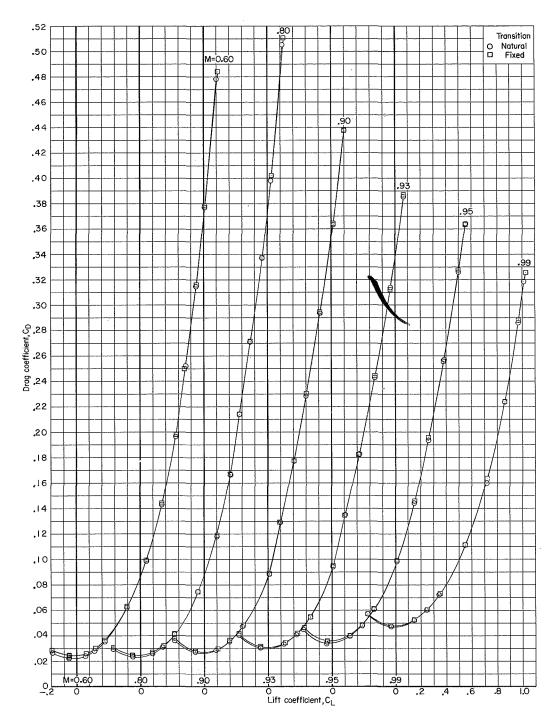
L-855

(d) Model configuration 3 plus wing inboard tanks and center-line-tank configuration B.

Figure 16.- Continued.
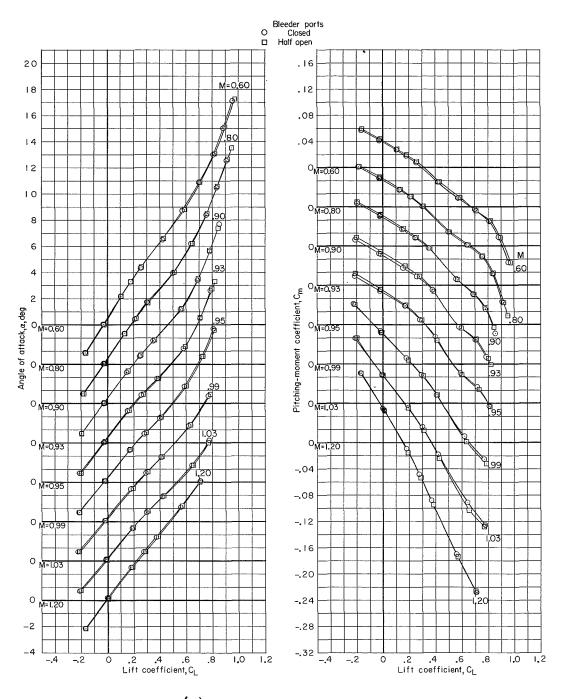
(d) Model configuration 3 plus wing inboard tanks and center-line-tank configuration B.  Concluded.

Figure 16.- Concluded.

Bleeder ports
O   Closed
□   Half open
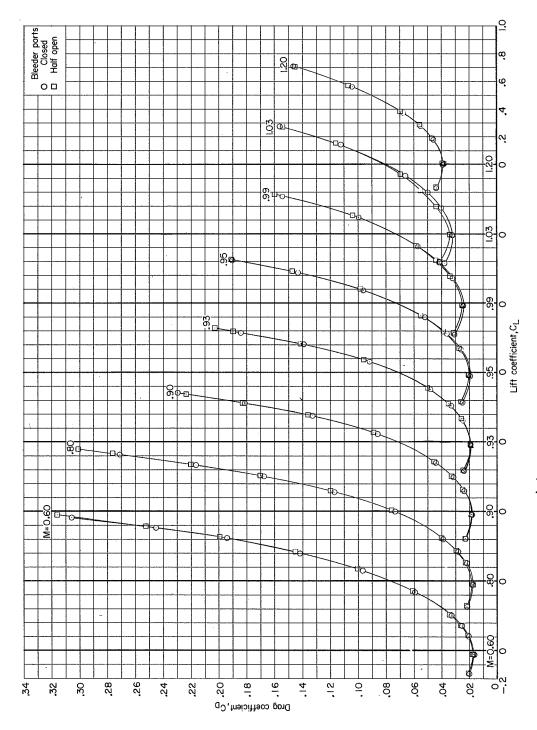


(a) Model configuration 3.

Figure 17.- Effect of inlet-duct bleeder ports on longitudinal
aerodynamic characteristics of several configurations.
$\delta_h$ = -3°;  8' TT.

(a) Model configuration 3.  Concluded.

Figure 17.- Continued.

Bleeder ports
O   Closed
□   Half open



(b) Model configuration 3 plus wing inboard tanks and center-line-tank configuration A.

Figure 17.- Continued.
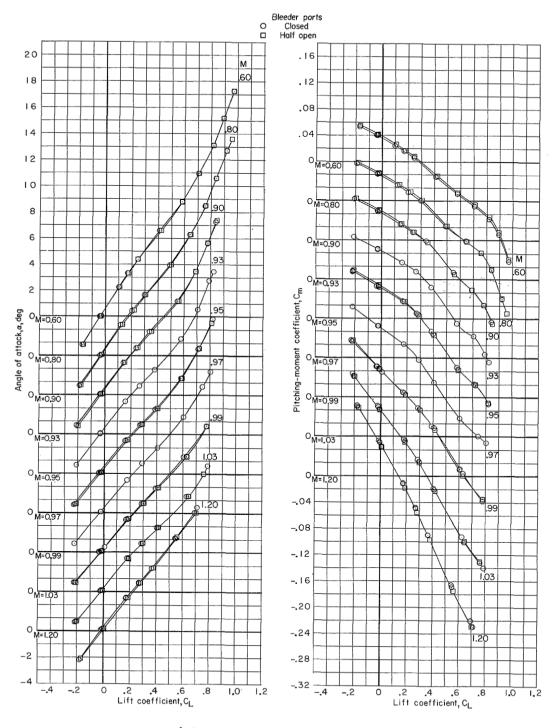
(b) Model configuration 3 plus wing inboard tanks and center-line-tank
configuration A.  Concluded.

Figure 17.- Continued.

55

L-855
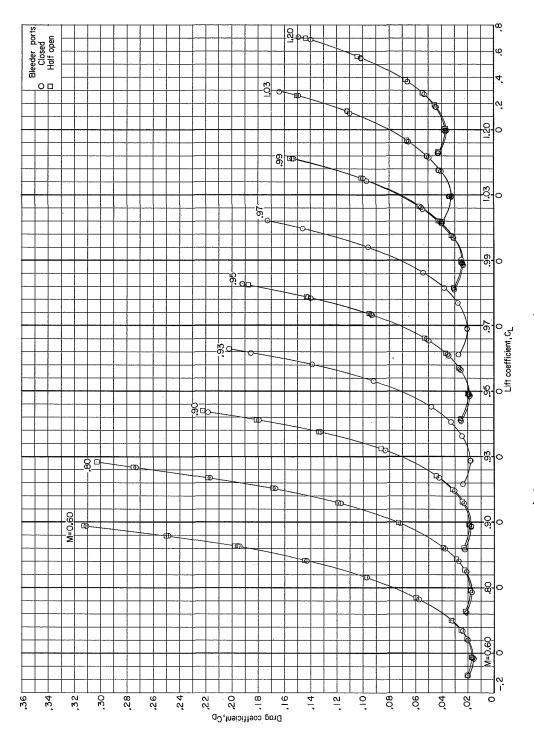


(c) Model configuration 4.

Figure 17.- Continued.
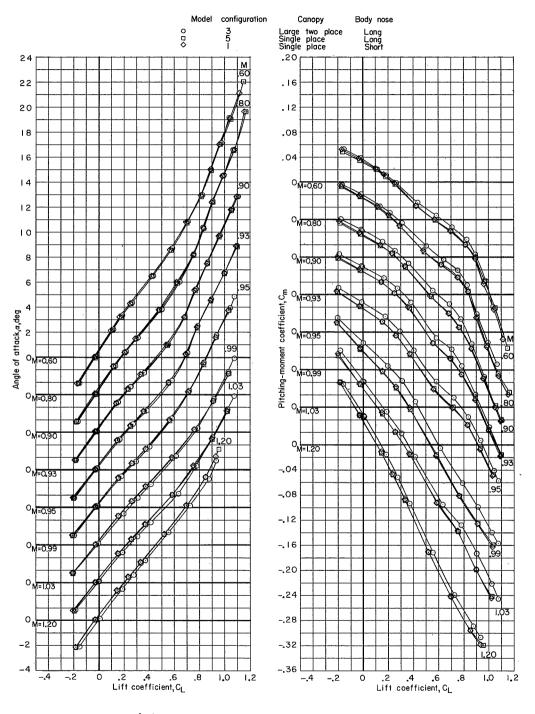
(c) Model configuration 4. Concluded.

Figure 17.- Concluded.

L-855

| Model configuration | Canopy | Body nose |
|---|---|---|
| ○  3 | Large two place | Long |
| □  5 | Single place | Long |
| ◇  1 | Single place | Short |

Angle of attack, α, deg

M .60 .80 .90 .95 .99 1.03 1.20

O M=0.60
O M=0.80
O M=0.90
O M=0.93
O M=0.95
O M=0.99
O M=1.03
O M=1.20

Lift coefficient, C_L

Pitching-moment coefficient, C_m

O M=0.60
O M=0.80
O M=0.90
O M=0.93
O M=0.95
O M=0.99
O M=1.03
O M=1.20

M 60 80 90 93 95 99 1.03 1.20

Lift coefficient, C_L
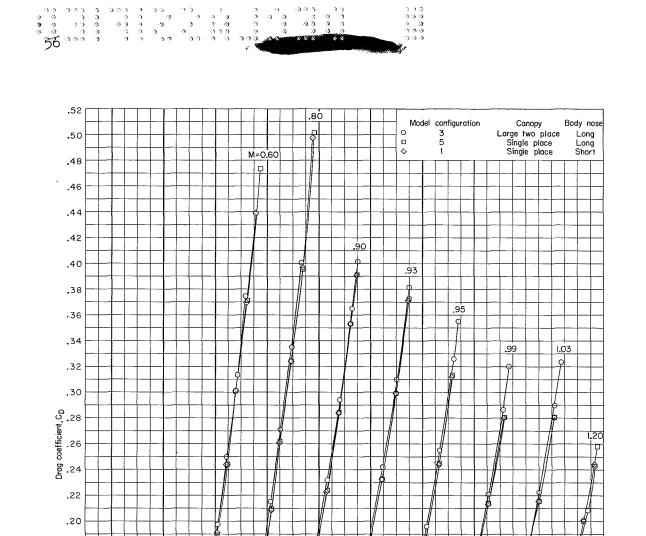
(a) Transition natural; 8' TPT.

Figure 18.- Effect of canopy and body-nose design on longitudinal aerodynamic characteristics. $\delta_h = -3^\circ$.

(a) Transition natural; 8' TPT. Concluded.

Figure 18.- Continued.

L-855
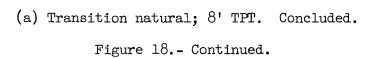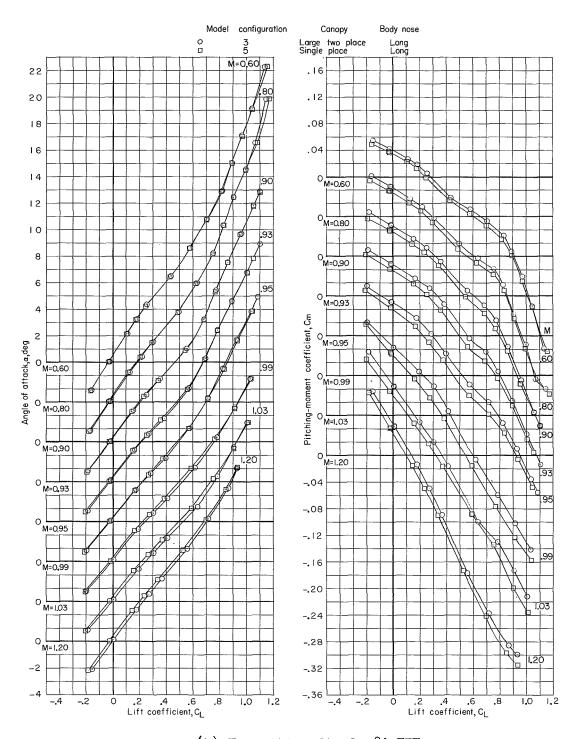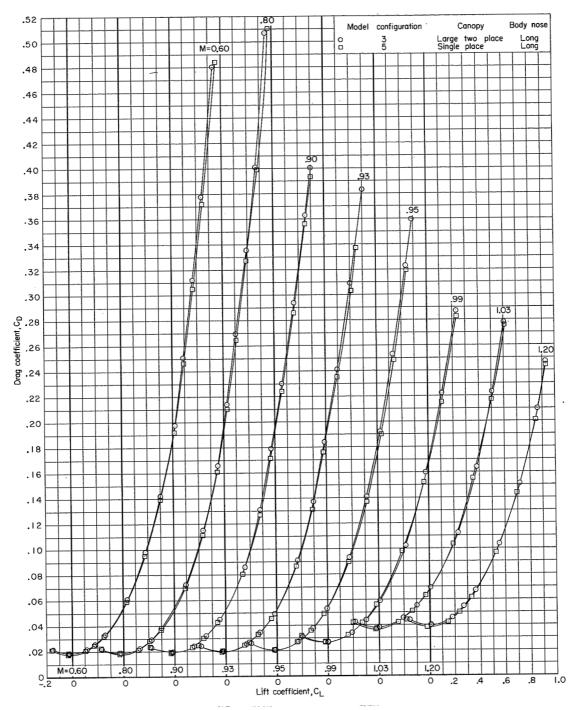
(b) Transition fixed; 8' TPT.

Figure 18.- Continued.

(b) Transition fixed; 8' TPT.  Concluded.

Figure 18.- Continued.

| Model configuration | | Canopy | | Body nose |
|---|---|---|---|---|
| ○ | 3 | Large two place | | Long |
| □ | 4 | Small two place | | Long |



(c) Inlet-duct bleeder ports half open; transition natural; 8' TT.
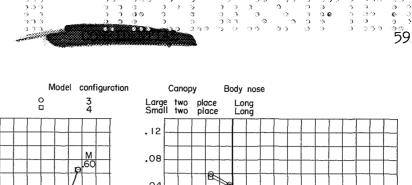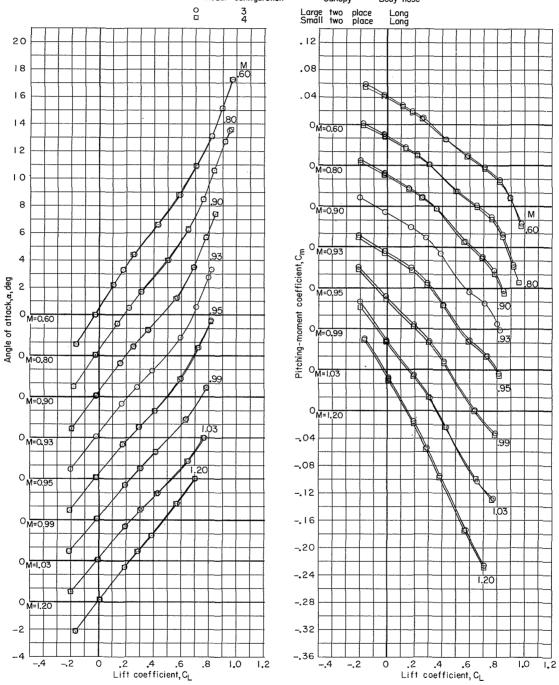
Figure 18.- Continued.

(c) Inlet-duct bleeder ports half open; transition natural; 8' TT. Concluded.

Figure 18.- Continued.

| Model configuration | | Canopy | Body nose |
|---|---|---|---|
| O | 1 | Single place | Short |
| ☐ | 2 | Large two place | Short |
| ◇ | 3 | Large two place | Long |
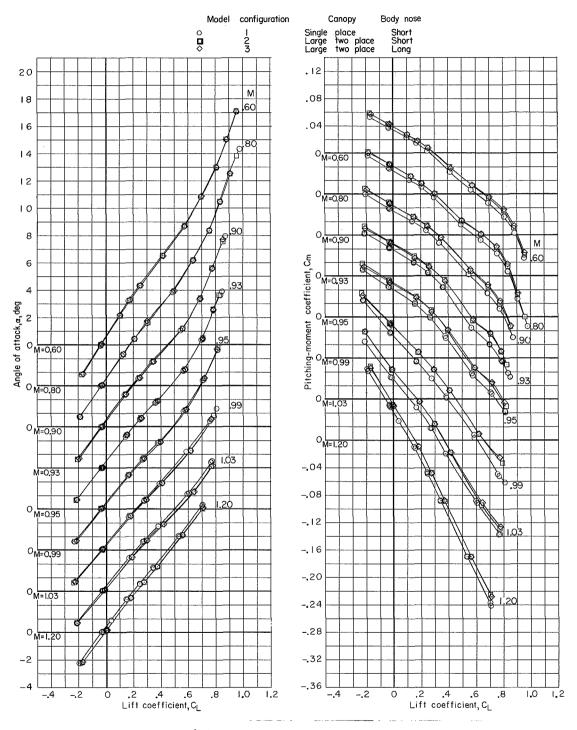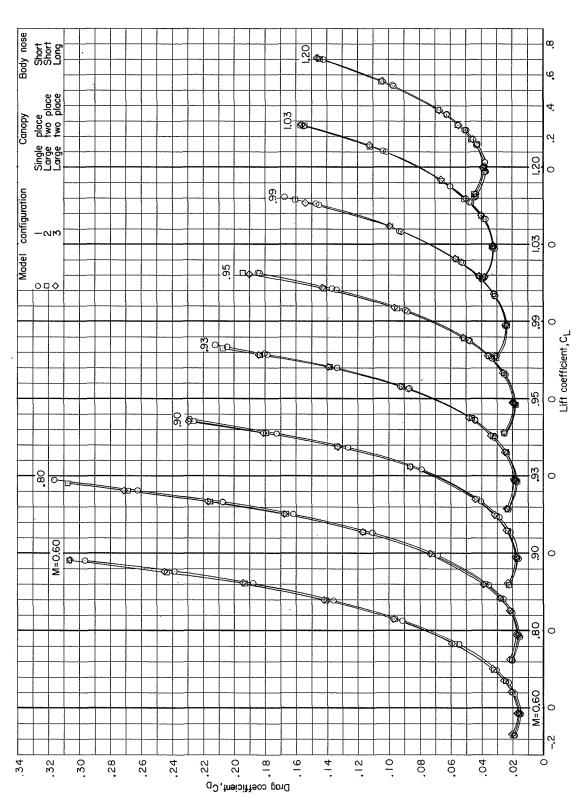


(d) Transition natural; 8' TT.

Figure 18.- Continued.

(d) Transition natural; 8' TT. Concluded.

Figure 18.- Concluded.

L-855

Body-nose boom
O    On
□    Off

Angle of attack, $\alpha$, deg

M

.60

.80

.90

.93

.95

.99

1.03

1.20

M=0.60

M=0.80

M=0.90

M=0.93

M=0.95

M=0.99

M=1.03

M=1.20

Lift coefficient, $C_L$

Pitching-moment coefficient, $C_m$

M=0.60

M=0.80

M=0.90

M=0.93

M=0.95

M=0.99

M=1.03

M=1.20

M
.60

.80

.90

.93

.95

.99

1.03

1.20

Lift coefficient, $C_L$
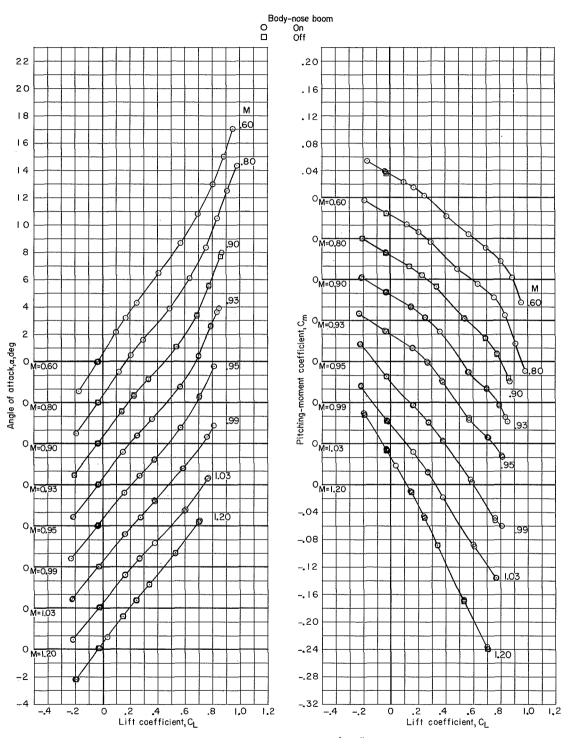
Figure 19.- Effect of body-nose boom on longitudinal aerodynamic characteristics of model configuration 1. $\delta_h = -3°$; 8' TT.
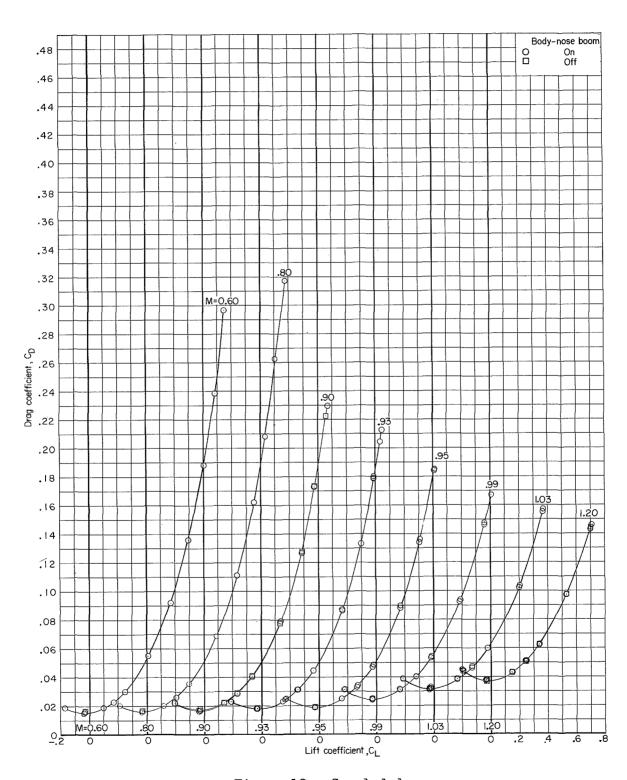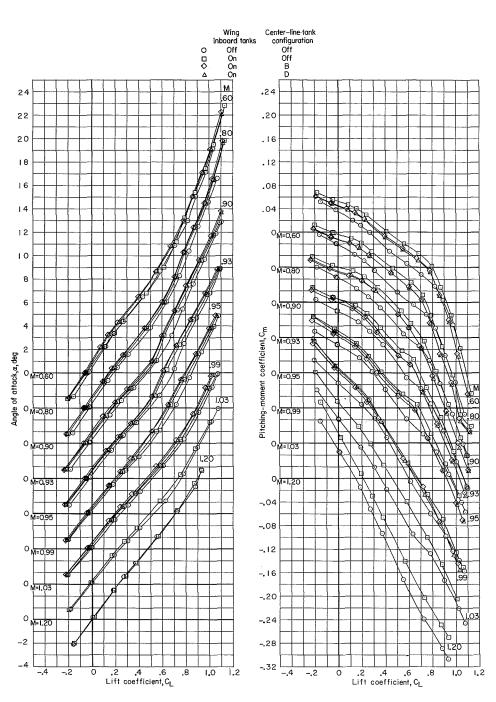
Figure 19.- Concluded.
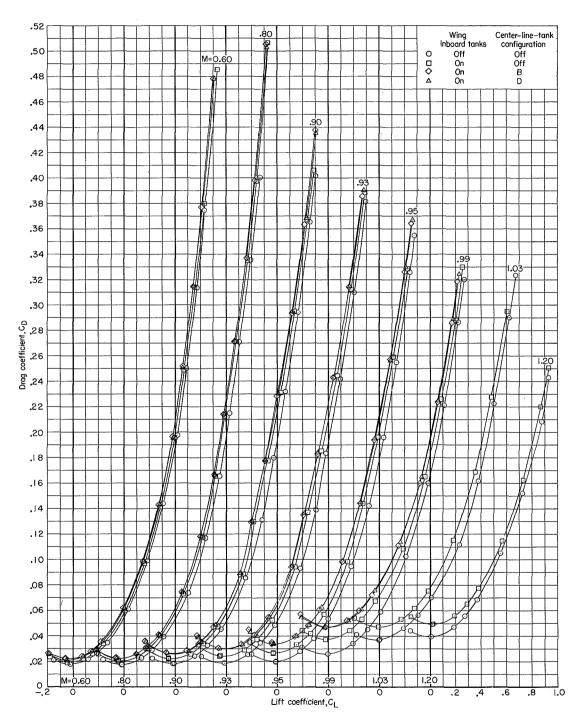
(a) Transition natural; 8' TPT.

Figure 20.- Effect of wing inboard tanks and center-line tanks on longitudinal aerodynamic characteristics of model configuration 3. $\delta_h = -3^\circ$.
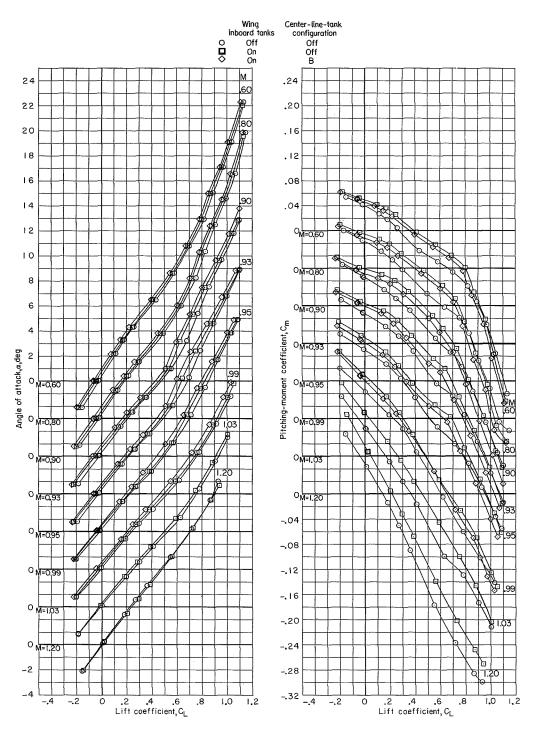
(a) Transition natural; 8' TPT.  Concluded.

Figure 20.- Continued.
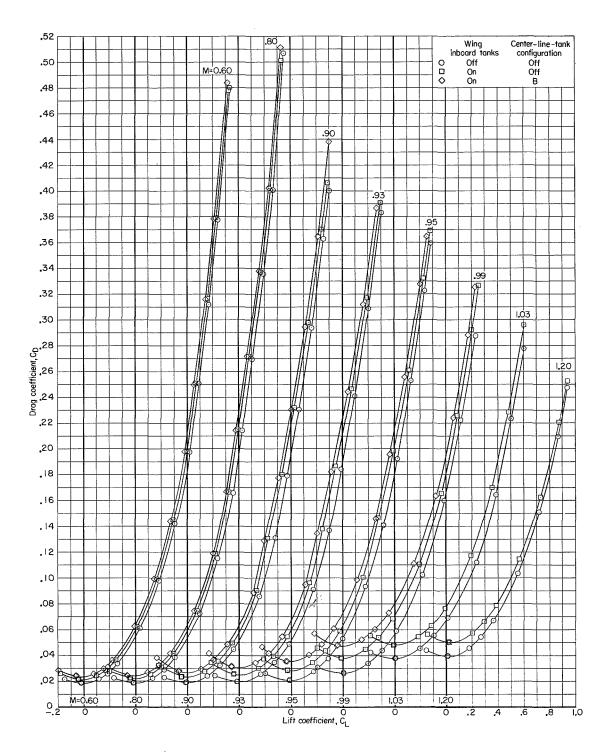
(b) Transition fixed; 8' TPT.

Figure 20.- Continued.

(b) Transition fixed; 8' TPT.  Concluded.

Figure 20.- Continued.

L-855
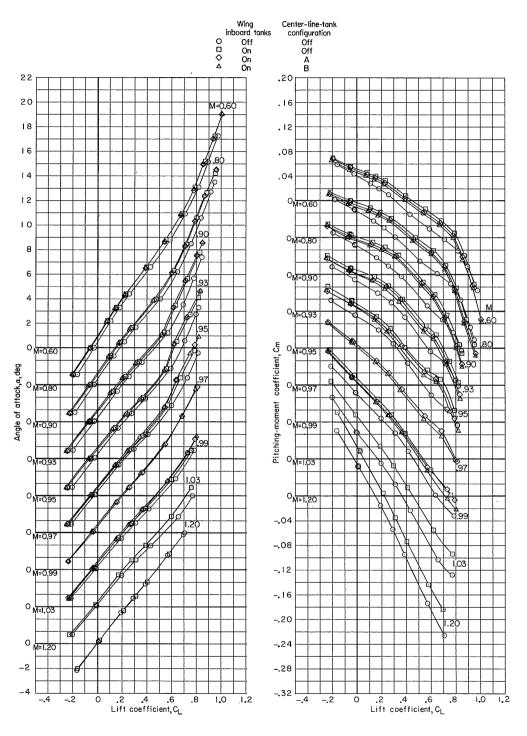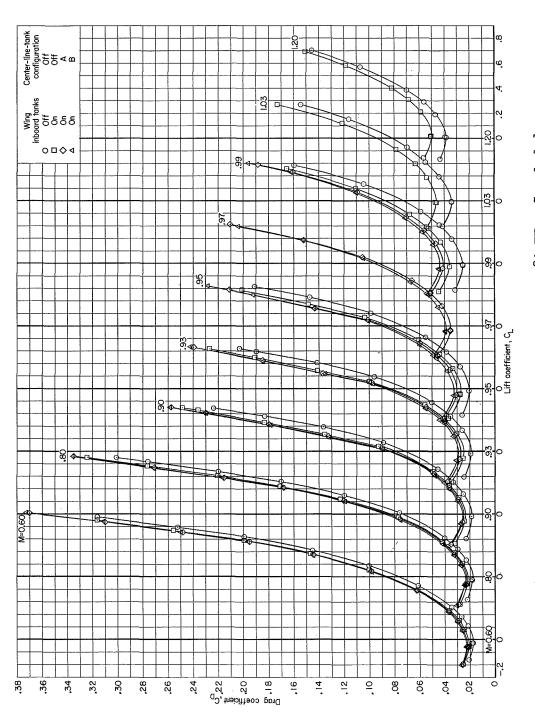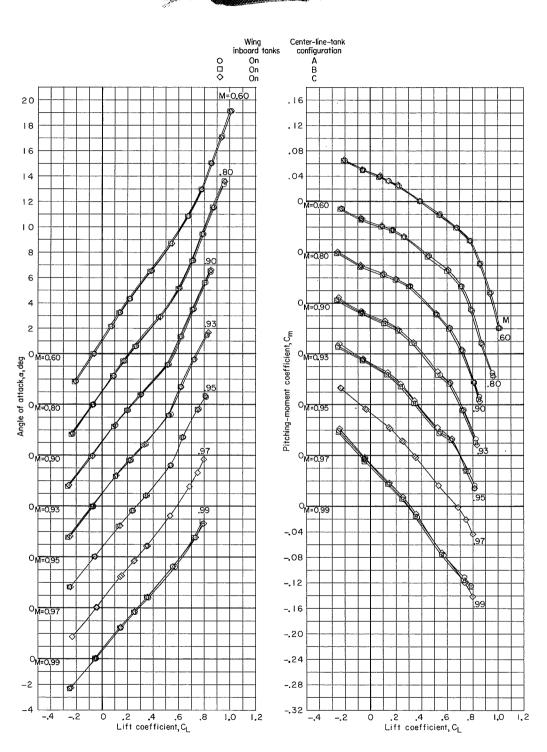
(c) Inlet-duct bleeder ports half open; 8' TT.

Figure 20.- Continued.

(c) Inlet-duct bleeder ports half open; 8' TT. Concluded.

Figure 20.- Continued.

L-855



| | Wing inboard tanks | Center-line-tank configuration |
|---|---|---|
| ○ | On | A |
| □ | On | B |
| ◇ | On | C |
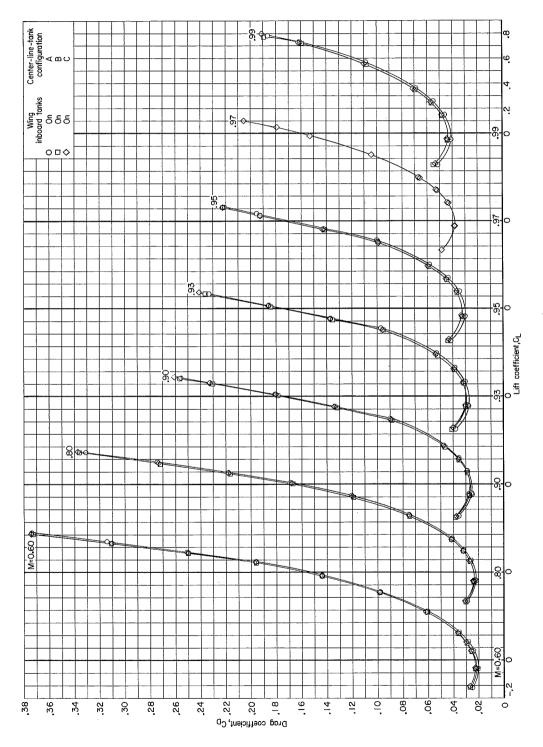
(d) Transition natural; 8' TT.

Figure 20.- Continued.

(d) Transition natural; 8' TT. Concluded.

Figure 20.- Concluded.

Wing-tip tanks
○   Off
□   Small
◇   Large
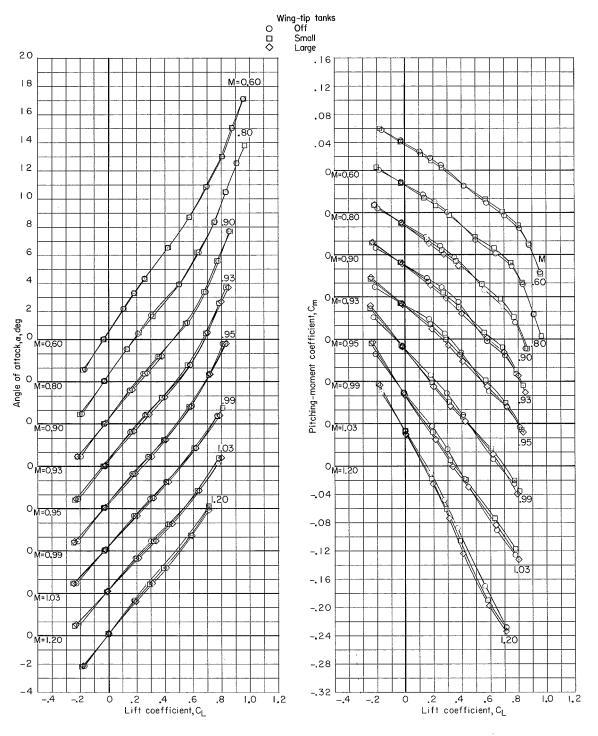


Figure 21.- Effect of wing-tip tanks on longitudinal aerodynamic characteristics of model configuration 3. $\delta_h$ = -3°; 8' TT.
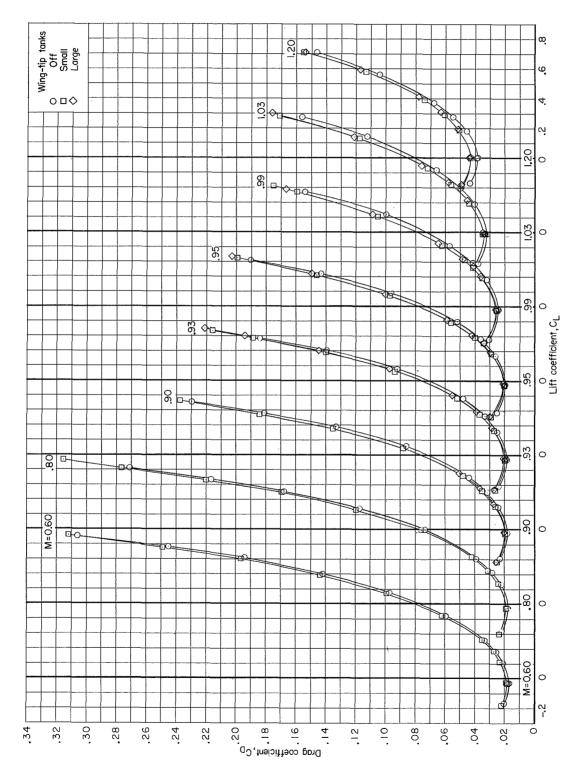
Figure 21.- Concluded.
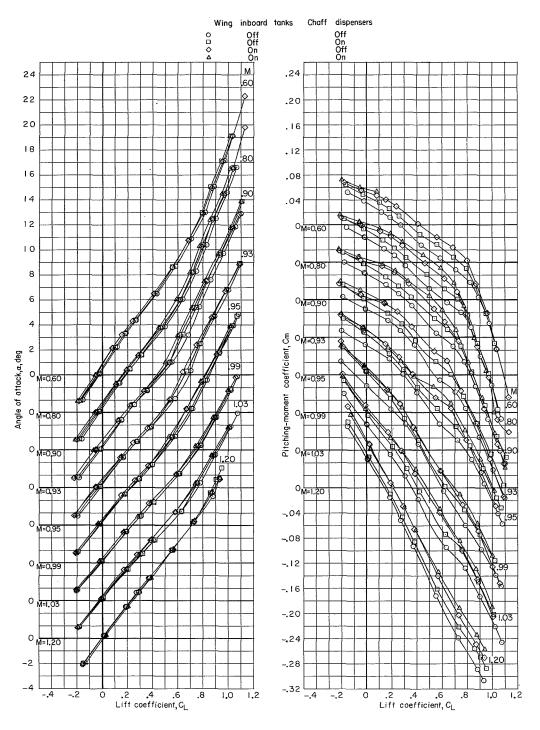
Figure 22.- Effect of chaff dispensers and wing inboard tanks on longitudinal aerodynamic characteristics of model configuration 3. $\delta_h$ = -3°; 8' TPT.

Figure 22.- Concluded.

Wing inboard pylons

o        Off
□        On
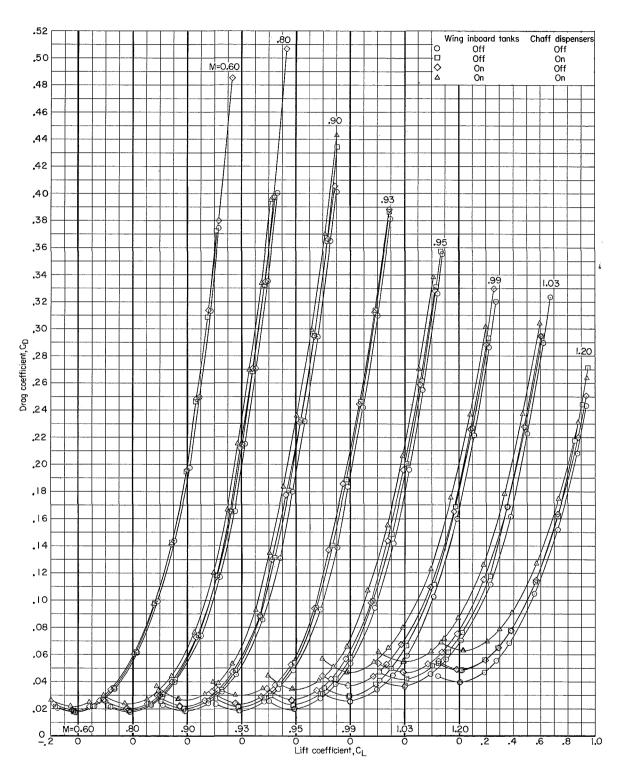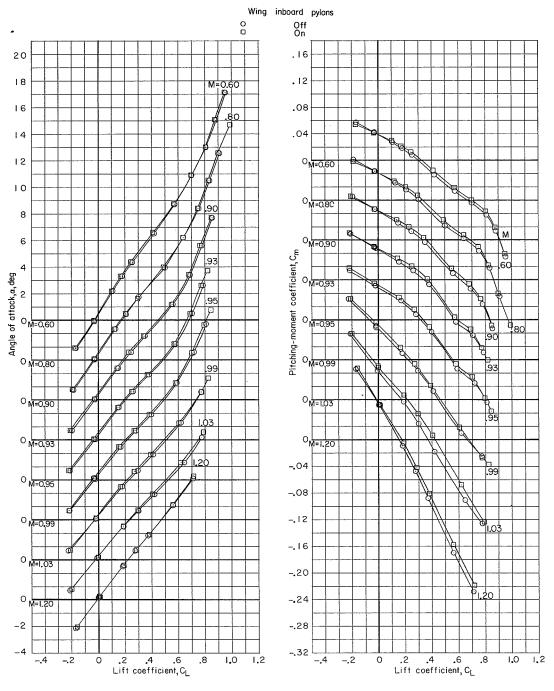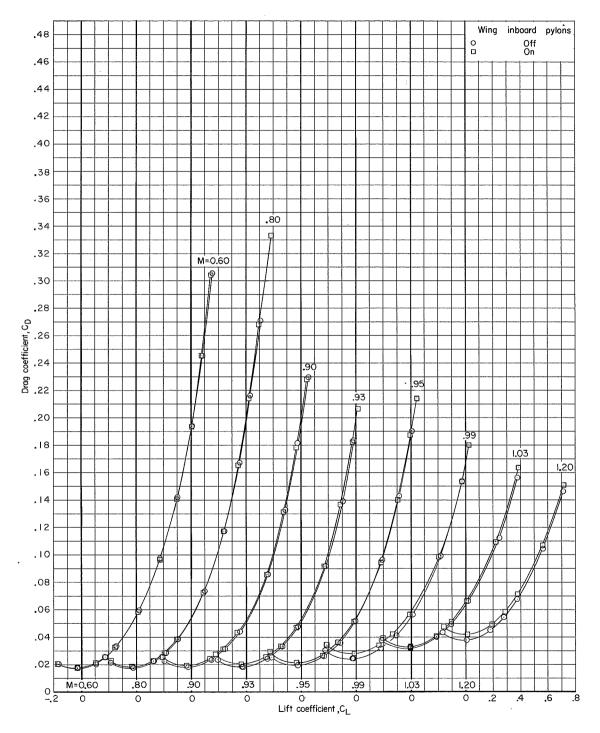


(a) Wing inboard pylons; 8' TT.

Figure 23.- Effect of wing pylons on longitudinal aerodynamic character-
istics of model configuration 3. $\delta_h$ = -3°.
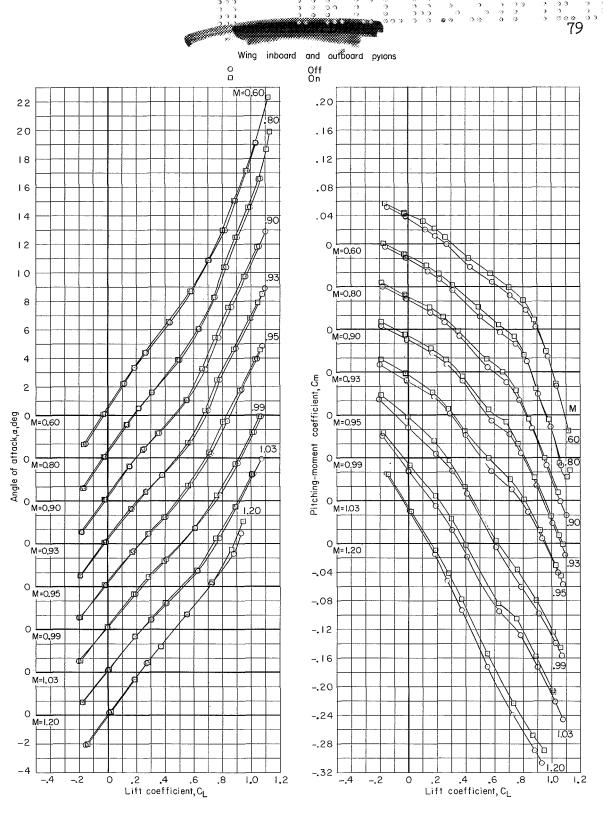
(a) Wing inboard pylons; 8' TT. Concluded.

Figure 23.- Continued.

L-855
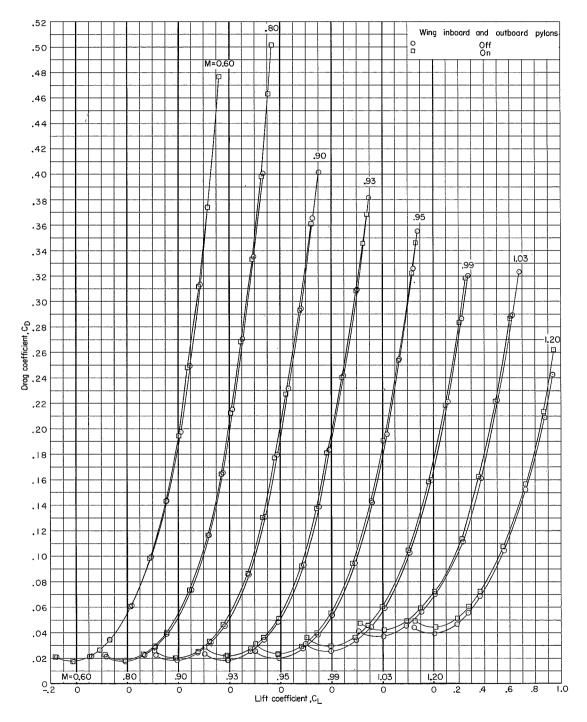


(b) Wing inboard and outboard pylons; 8' TPT.

Figure 23.- Continued.

(b) Wing inboard and outboard pylons; 8' TPT.  Concluded.

Figure 23.- Concluded.

L-855
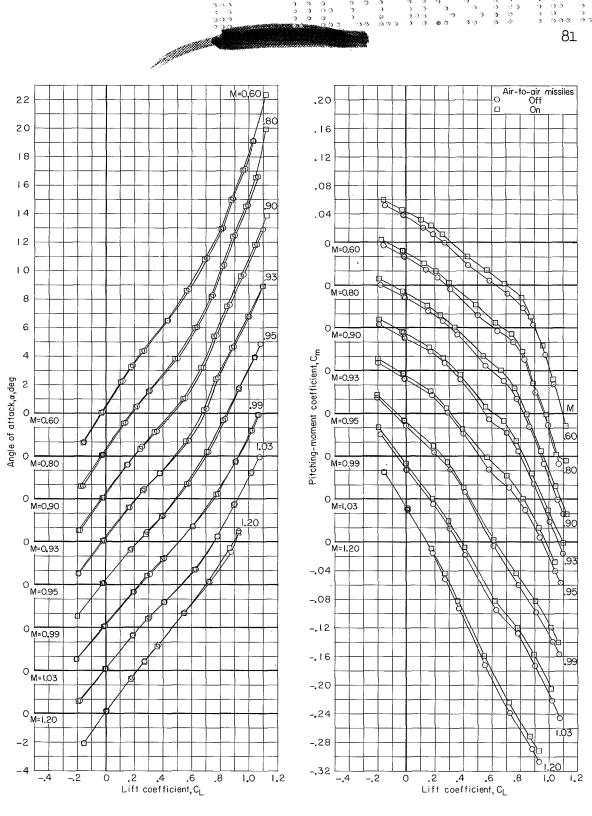


Figure 24.- Effect of air-to-air missiles on longitudinal aerodynamic characteristics of model configuration 3.   $\delta_h$ = -3°.
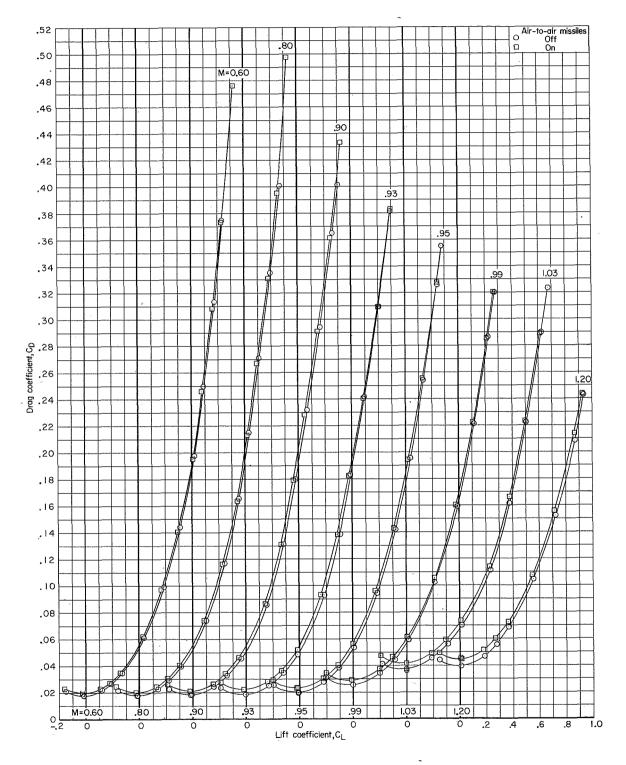
Figure 24.- Concluded.

| Afterbody bump (fuel) | Exit-nozzle blisters |
|---|---|
| O  Off | Off |
| □  Off | On |
| ◇  On | Off |
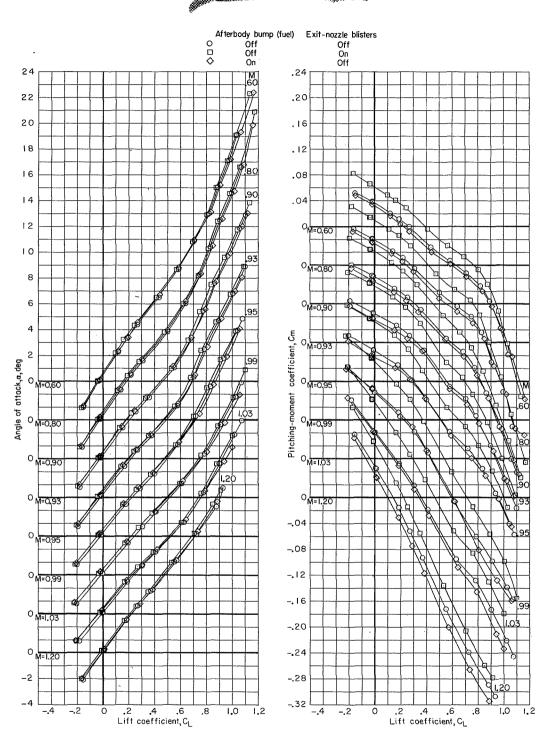


Figure 25.- Effect of afterbody bump (for fuel storage) and exit-nozzle blisters on longitudinal aerodynamic characteristics of model configuration 3. $\delta_h = -3°$; 8' TPT.

| Afterbody bump (fuel) | Exit-nozzle blisters |
|---|---|
| ○ Off | Off |
| □ Off | On |
| ◇ On | Off |
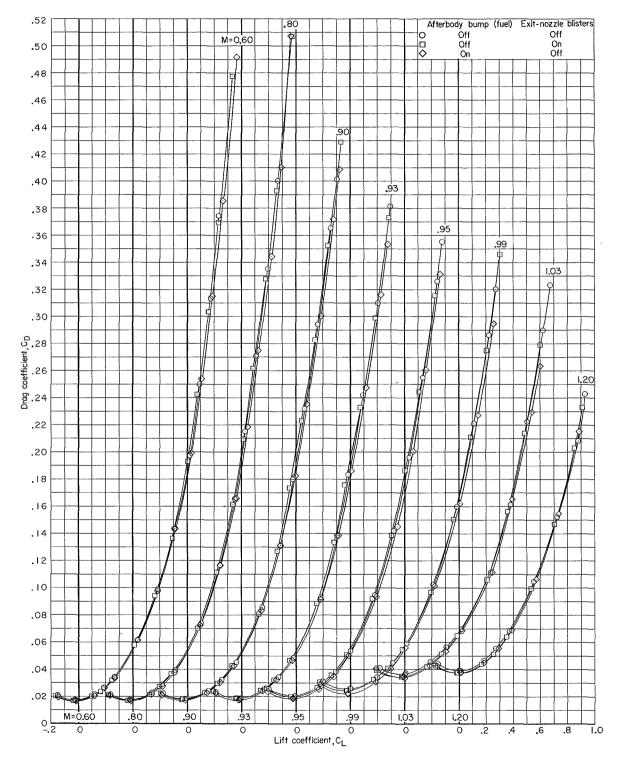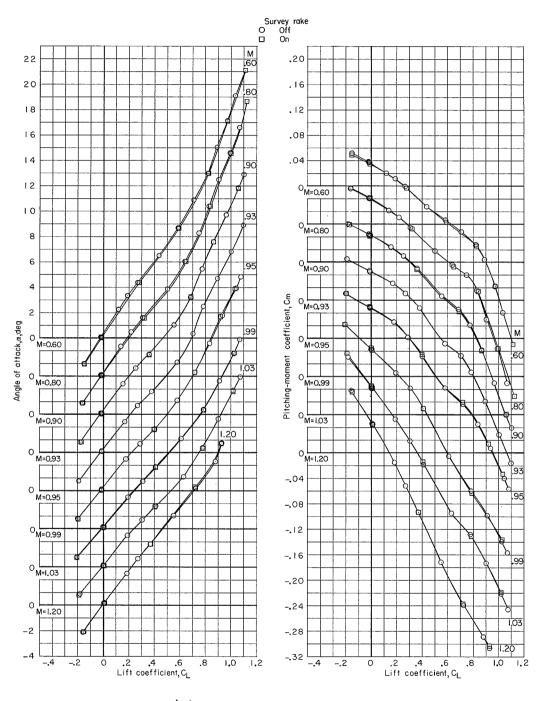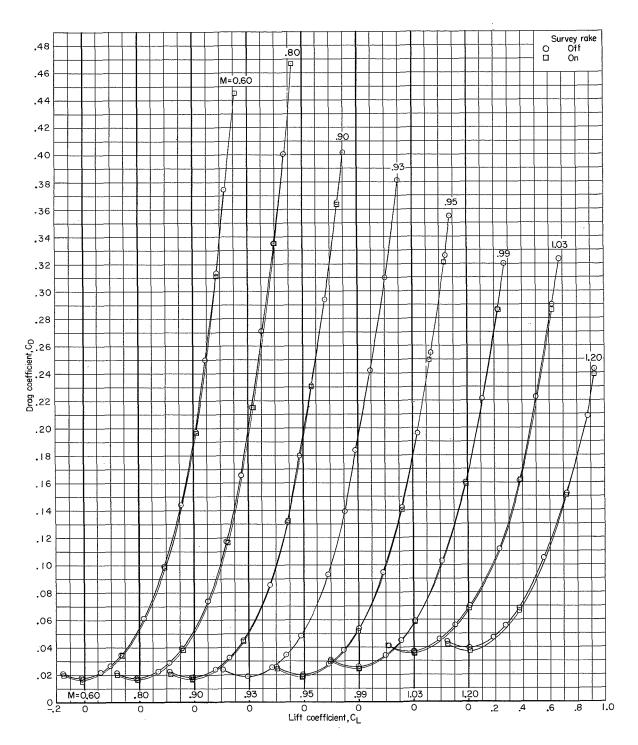
Figure 25.- Concluded.
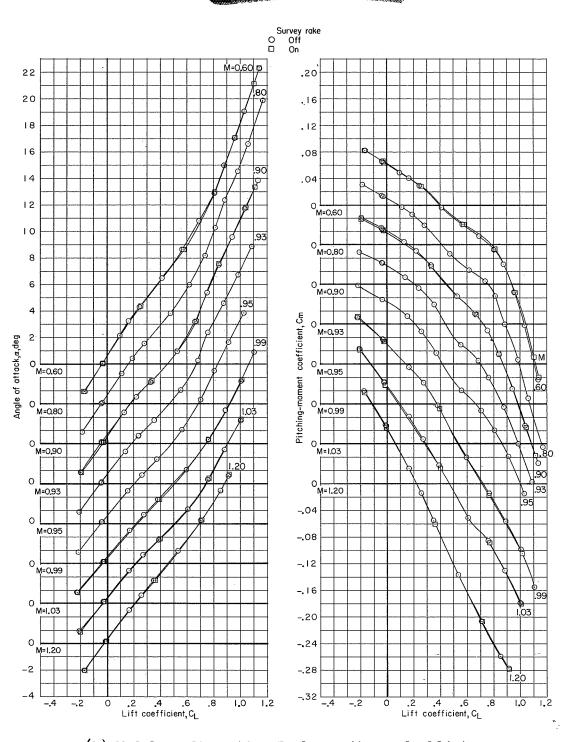
(a) Model configuration 3. Concluded.

Figure 26.- Continued.

L-855
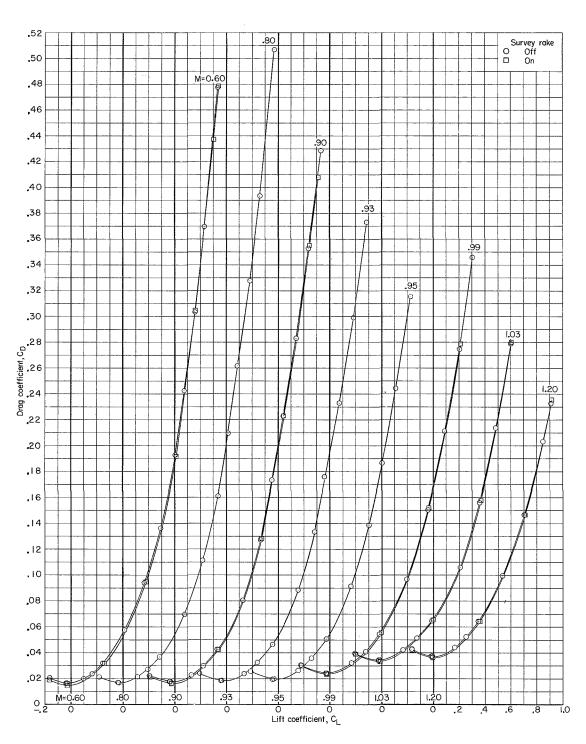


(b) Model configuration 3 plus exit-nozzle blisters.

Figure 26.- Continued.

(b) Model configuration 3 plus exit-nozzle blisters.  Concluded.

Figure 26.- Concluded.

Duct exit area, sq in.
○  2.024
□  1.507
◇  1.109
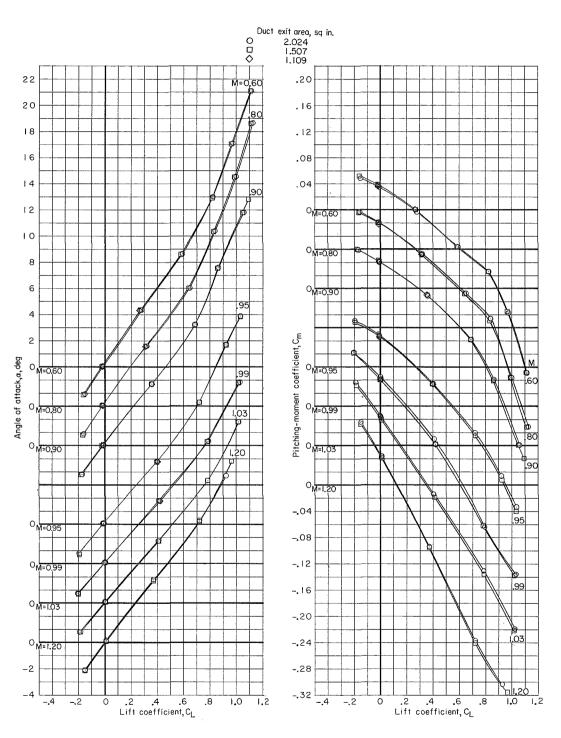


Figure 27.- Effect of duct exit area on longitudinal aerodynamic charac-
teristics of model configuration 3 plus survey rake.  $\delta_h = -3°$;
8' TPT.
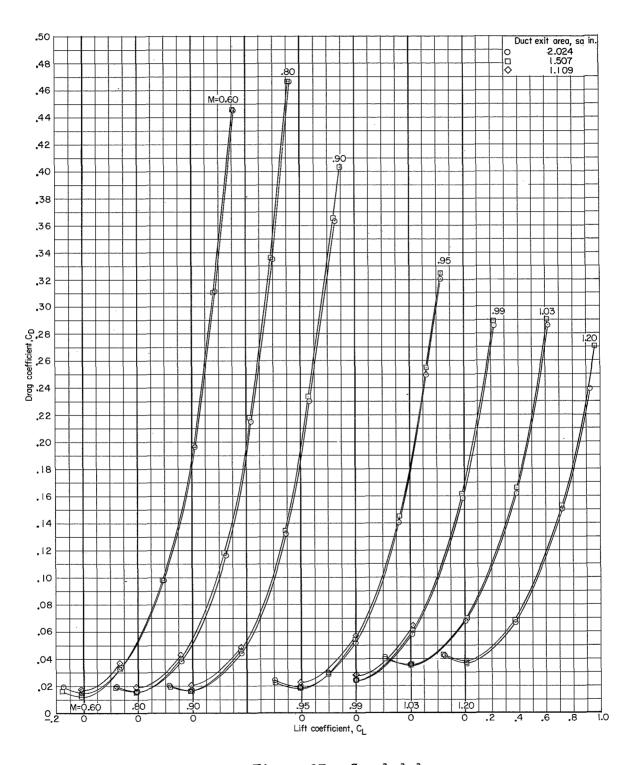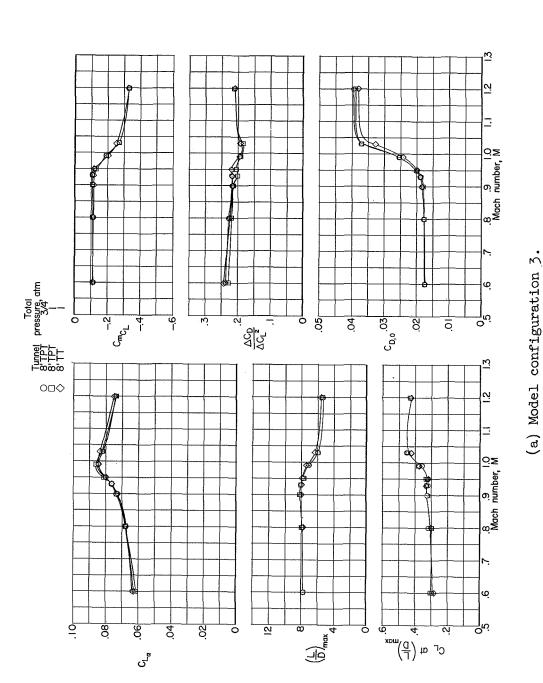
Figure 27.- Concluded.
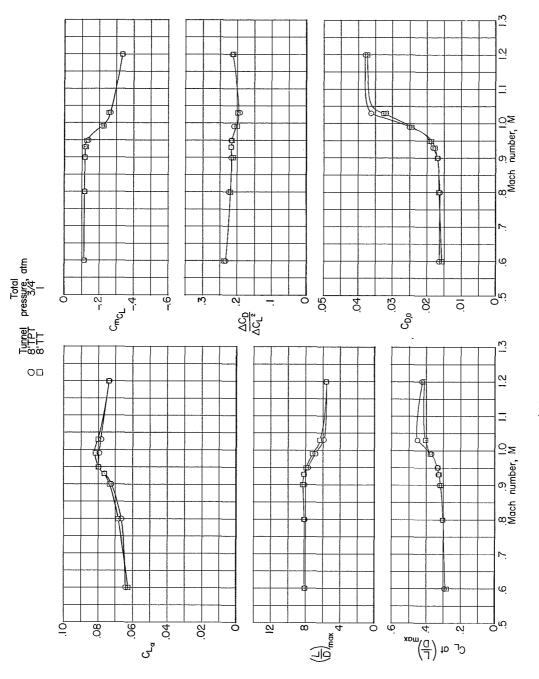
(a) Model configuration 3.

Figure 28.- Comparison of performance and longitudinal-stability derivatives of several configurations tested in both the 8' TPT and the 8' TT. $\delta_h = -3°$.
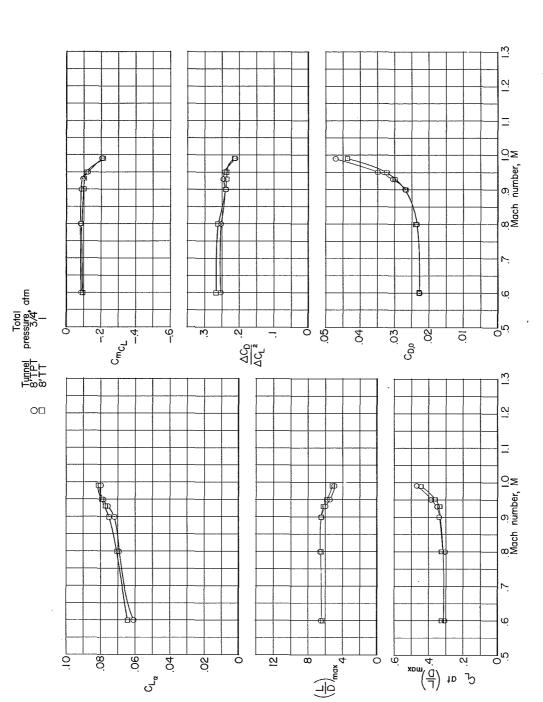
(b) Model configuration 1.

Figure 28.- Continued.
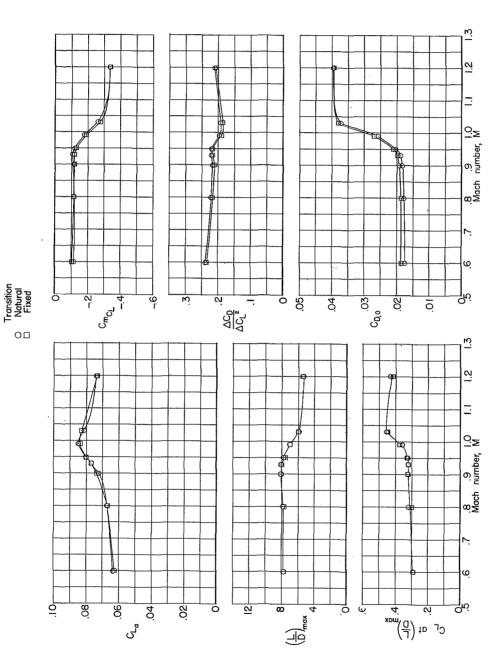
L-855

Total
pressure, atm
Tunnel   3/4   1
O  8'TPT
□  8'TT

$C_{m_{C_L}}$

0
-.2
-.4
-.6

$\dfrac{\Delta C_D}{\Delta C_L{}^2}$

.3
.2
.1
0

$C_{D,0}$

.05
.04
.03
.02
.01
0

Mach number, M

.5  .6  .7  .8  .9  1.0  1.1  1.2  1.3

$C_{L_\alpha}$

.10
.08
.06
.04
.02
0

$\left(\dfrac{L}{D}\right)_{max}$

12
8
4
0

$C_L$ at $\left(\dfrac{L}{D}\right)_{max}$

.6
.4
.2
0

Mach number, M

.5  .6  .7  .8  .9  1.0  1.1  1.2  1.3

(c) Model configuration 3 plus wing inboard tanks and center-line-tank configuration B.

Figure 28.- Concluded.

Transition
Natural
Fixed

$C_{m_{C_L}}$

$\dfrac{\Delta C_D}{\Delta C_L^2}$

$C_{D,o}$

$C_{L_\alpha}$

$\left(\dfrac{L}{D}\right)_{max}$

$C_L$ at $\left(\dfrac{L}{D}\right)_{max}$

Mach number, M
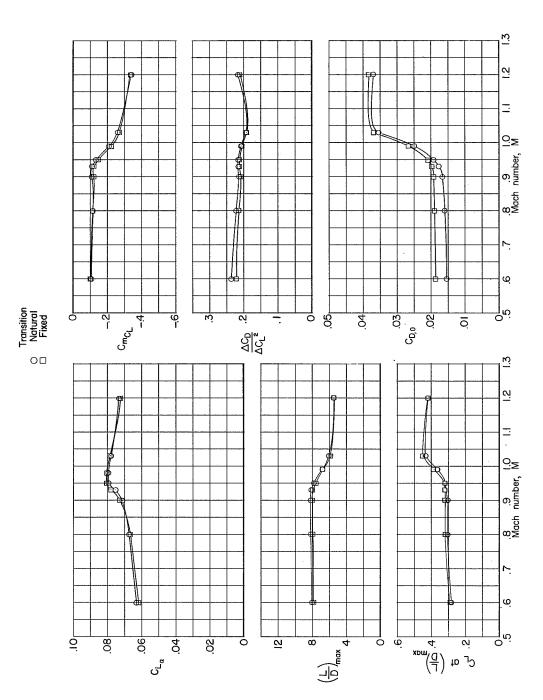
(a) Model configuration 3.

Figure 29.- Effect of fixed transition on performance and longitudinal-stability derivatives of several configurations. $\delta_h = -3°$; 8' TPT.

L-855
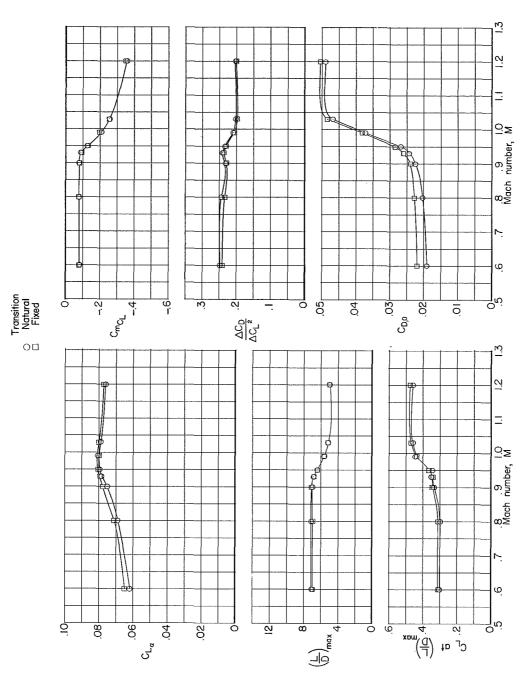
(b) Model configuration 5.

Figure 29.- Continued.
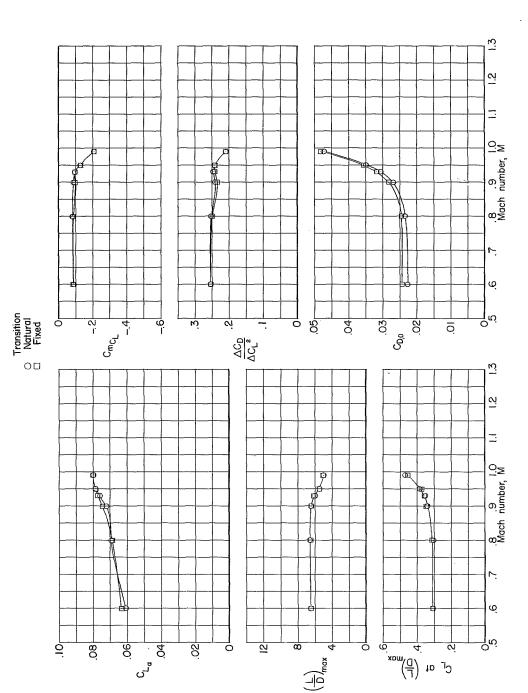
(c) Model configuration 3 plus wing inboard tanks.

Figure 29.- Continued.
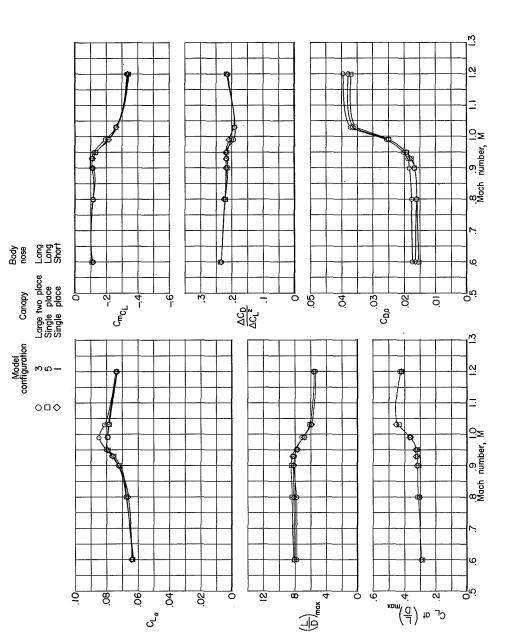
Transition
○ Natural
□ Fixed

$C_{m_{C_L}}$

$\dfrac{\Delta C_D}{\Delta C_L^{\,2}}$

$C_{D,0}$

Mach number, M

$C_{L_\alpha}$

$\left(\dfrac{L}{D}\right)_{max}$

$C_L$ at $\left(\dfrac{L}{D}\right)_{max}$

Mach number, M

(d) Model configuration 3 plus wing inboard tanks and center-line-tank configuration B.
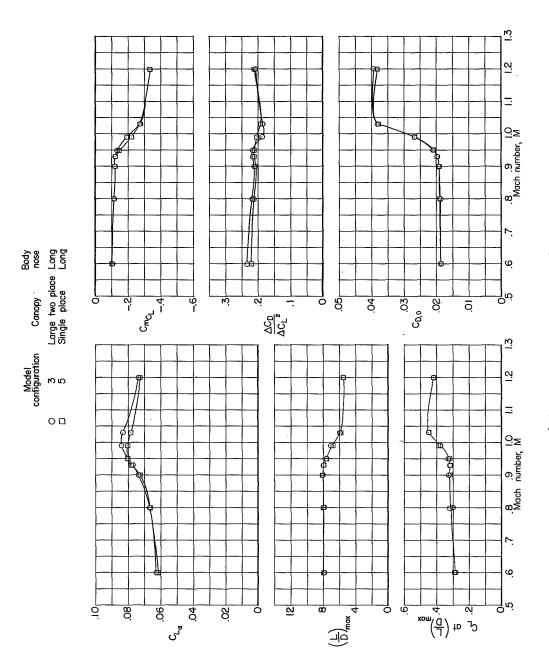
Figure 29.- Concluded.

(a) Transition natural; 8' TPT.

Figure 30.- Effect of canopy and body-nose design on performance and longitudinal-stability derivatives. $\delta_h = -3°$.
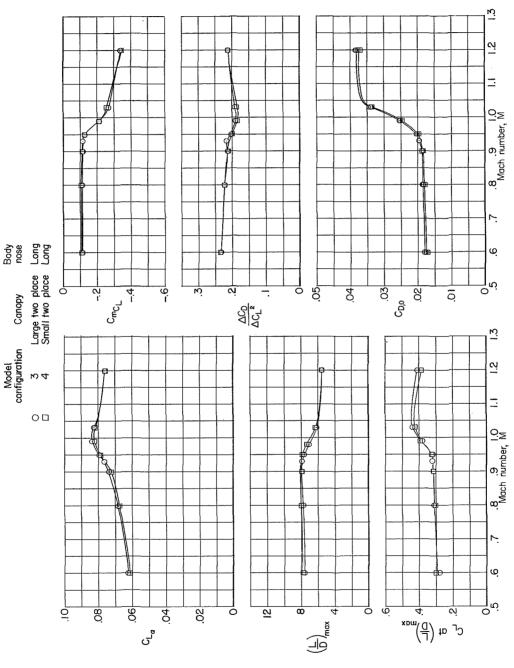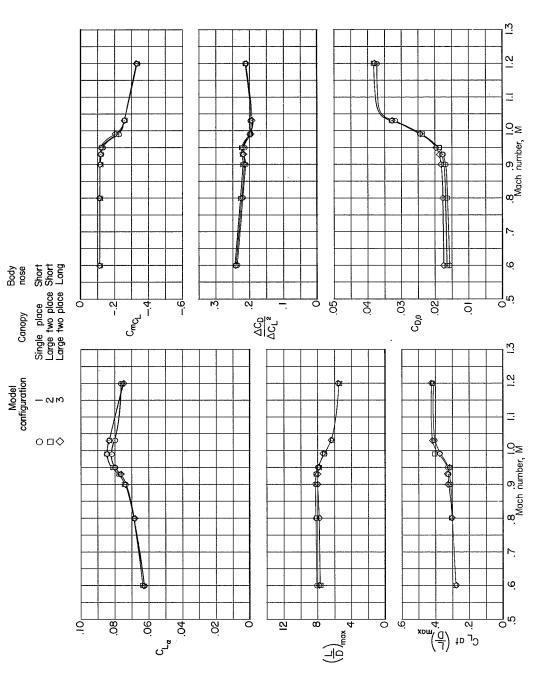
L-855



| Model configuration | Canopy | Body nose |
|---|---|---|
| O  3 | Large two place | Long |
| □  5 | Single place | Long |

(b) Transition fixed; 8' TPT.

Figure 30.- Continued.

(c) Inlet-duct bleeder ports half open; transition natural; 8' TT.

Figure 30.- Continued.

L-855

| Model configuration | | Canopy | Body nose |
|---|---|---|---|
| 1 | O | Single place | Short |
| 2 | □ | Large two place | Short |
| 3 | ◇ | Large two place | Long |

$C_{m_{C_L}}$

$\dfrac{\Delta C_D}{\Delta C_L^{\,2}}$

$C_{D,0}$

$C_{L_\alpha}$

$\left(\dfrac{L}{D}\right)_{max}$

$C_L$ at $\left(\dfrac{L}{D}\right)_{max}$

Mach number, M

(d) Transition natural; 8' TT.

Figure 30.- Concluded.

(a) Transition natural; 8' TPT.
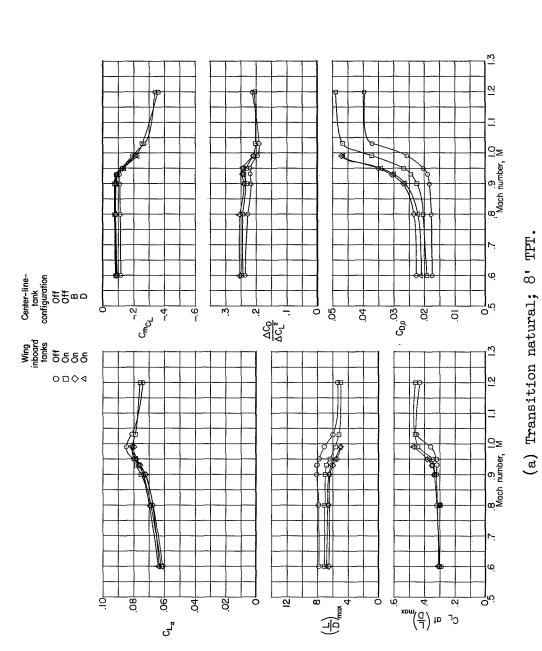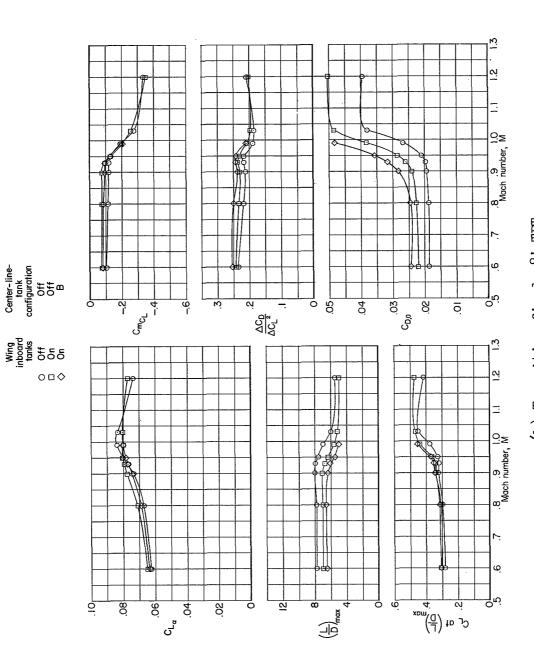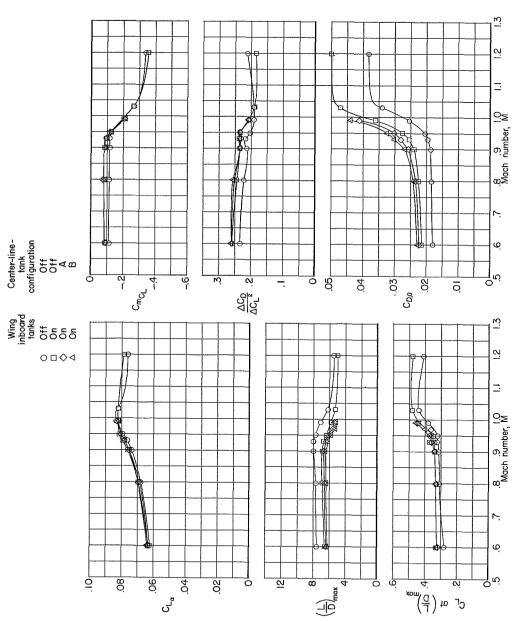
Figure 31.- Effect of wing inboard tanks and center-line tanks on performance and longitudinal-stability derivatives of model configuration 3.   $\delta_h = -3°$.

L-855



(b) Transition fixed; 8' TPT.

Figure 31.- Continued.
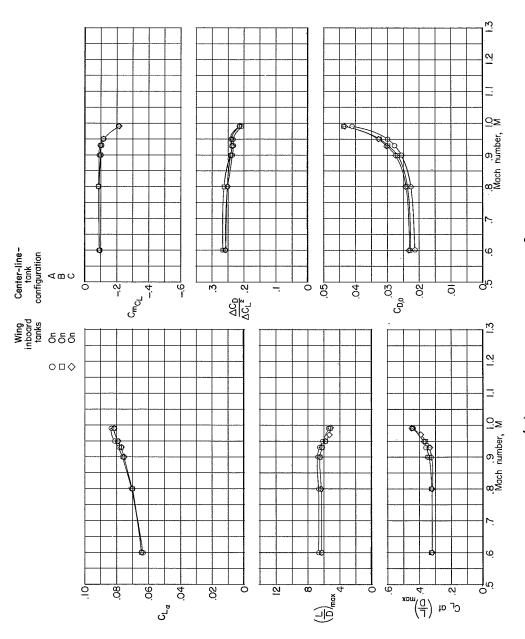
(c) Transition natural; inlet-duct bleeder ports half open; 8' TT.

Figure 31.- Continued.

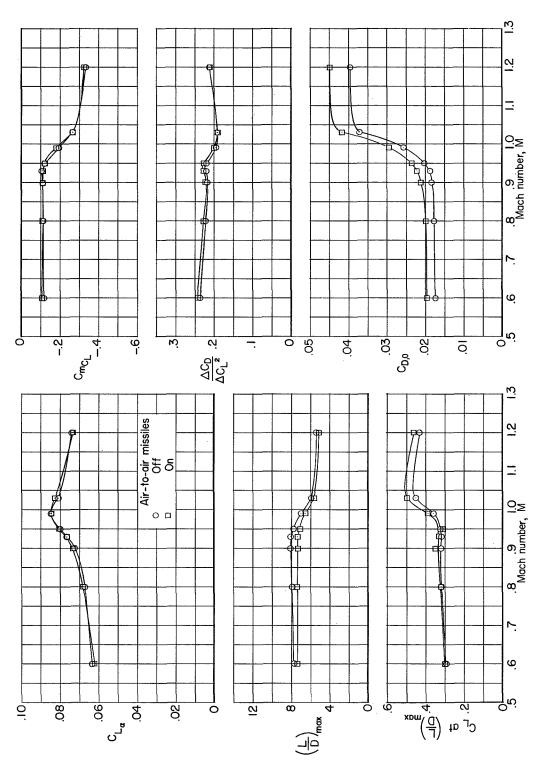L-855



(d)  Transition natural;  8' TT.

Figure 31.- Concluded.
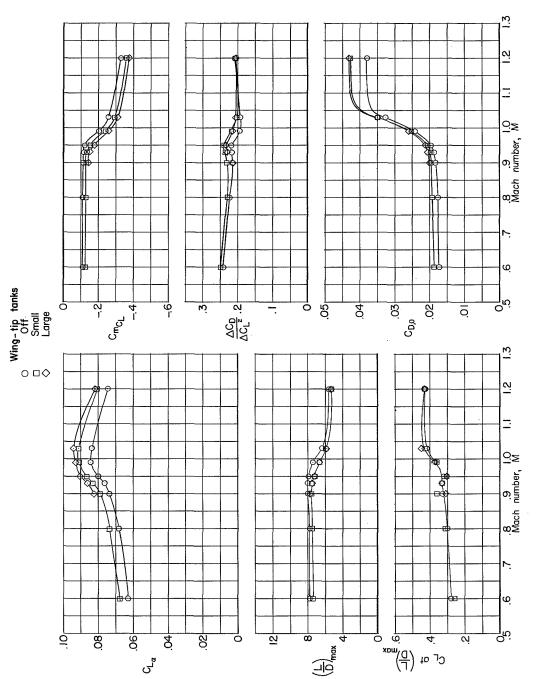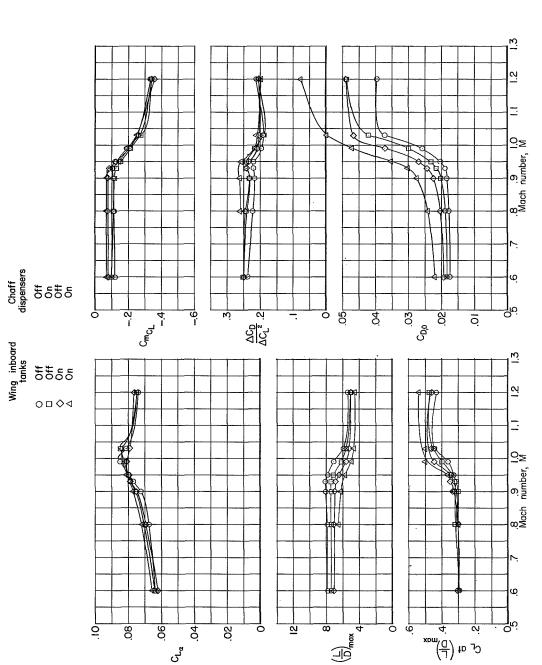
Figure 32.- Effect of wing-tip tanks on performance and longitudinal-stability derivatives of model configuration 3. $\delta_h = -3°$; 8' TT.
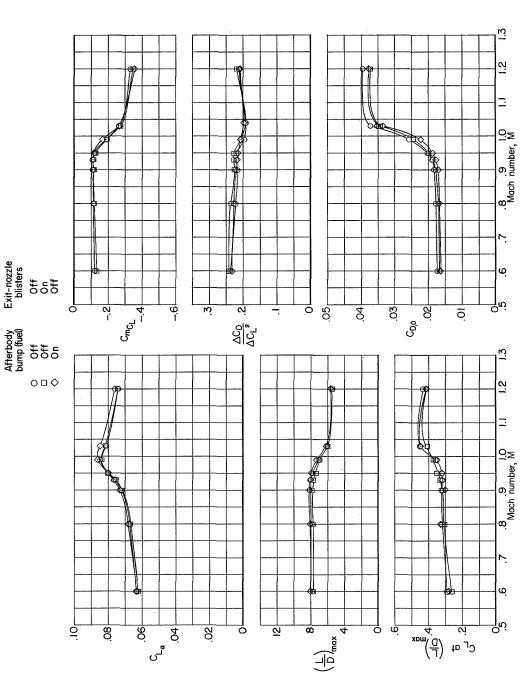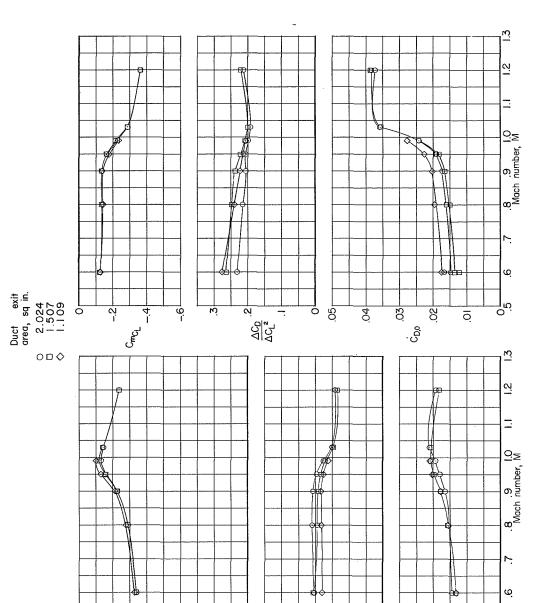
Figure 33.- Effect of chaff dispensers and wing inboard tanks on performance and longitudinal-stability derivatives of model configuration 3. $\delta_h = -3°$; 8' TPT.

(a) Wing inboard pylons; 8' TT.
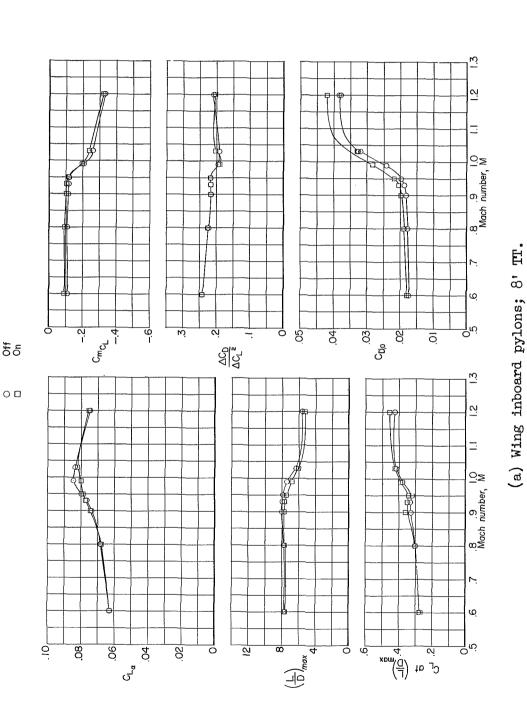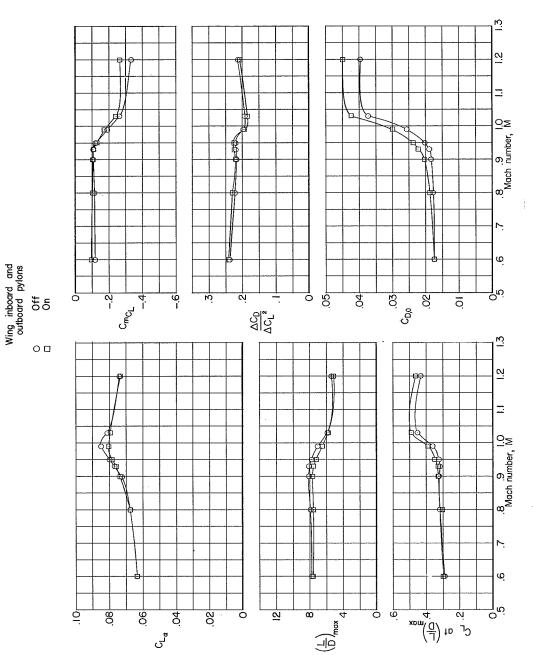
Figure 34.- Effect of wing pylons on performance and longitudinal-stability derivatives of model configuration 3. $\delta_h = -3°$.

L-855



(b), Wing inboard and outboard pylons; 8' TPT.

Figure 34.- Concluded.

Figure 35.- Effect of air-to-air missiles on performance and longitudinal-stability derivatives of model configuration 3. $\delta_h = -3°$; 8' TPT.

L-855



Figure 36.- Effect of afterbody bump (for fuel storage) and exit-nozzle blisters on performance and longitudinal-stability derivatives of model configuration 3. $\delta_h = -3°$; 8' TPT.

Figure 37.- Effect of duct exit area on performance and longitudinal-stability derivatives of model configuration 3 plus survey rake. $\delta_h = -3°$; 8' TPT.
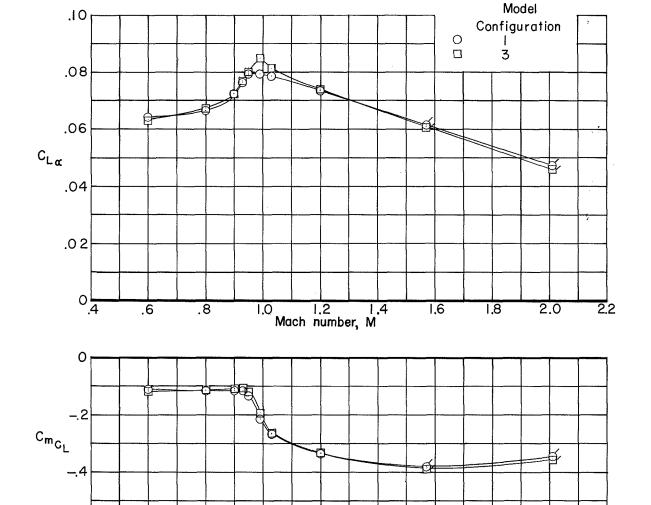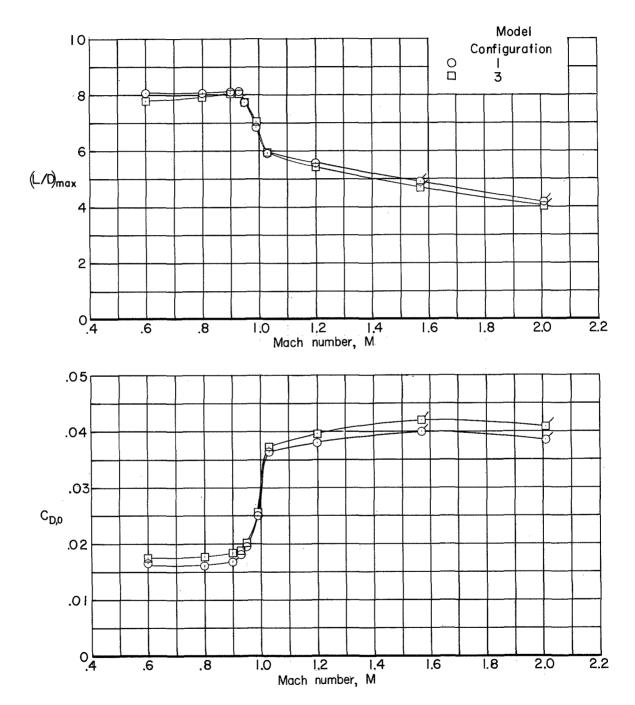
(a)  $C_{L_{\alpha}}$  and  $C_{m_{C_L}}$  plotted against  M.

Figure 38.- Effect of Mach number on performance and longitudinal-
stability derivatives of model configurations 1 and 3.  $\delta_h = -3°$;
(Flagged symbols indicate data points from ref. 1.)

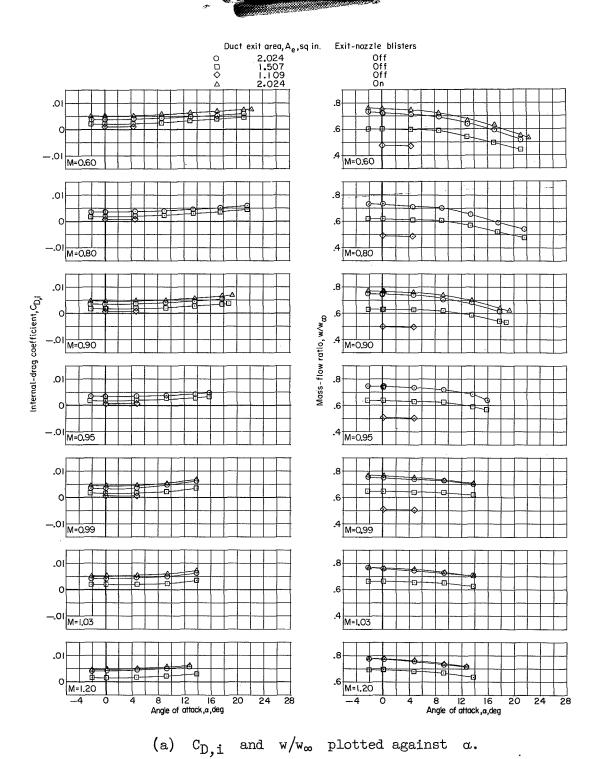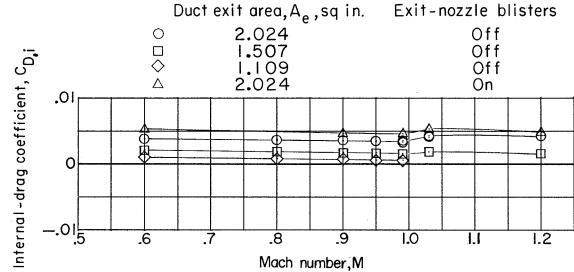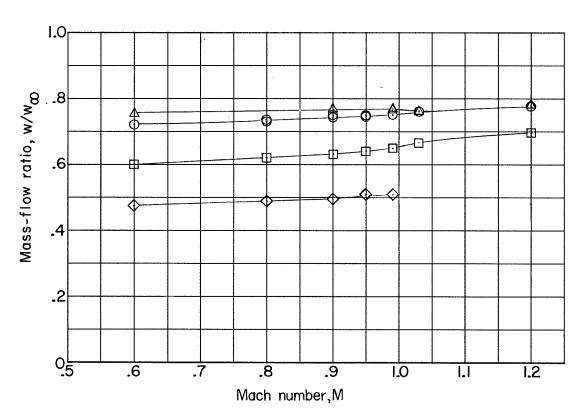(b)  $(L/D)_{max}$  and  $C_{D,o}$  plotted against  M.

Figure 38.- Concluded.

| Duct exit area, $A_e$, sq in. | Exit-nozzle blisters |
|---|---|
| ○ 2.024 | Off |
| □ 1.507 | Off |
| ◇ 1.109 | Off |
| △ 2.024 | On |



(a)  $C_{D,i}$  and  $w/w_\infty$  plotted against  $\alpha$.

Figure 39.- Internal-drag coefficient and mass-flow ratio of model configuration 3.  $\delta_h = -3°$; 8' TPT.

Duct exit area, $A_e$, sq in.    Exit-nozzle blisters

| | | |
|---|---|---|
| ○ | 2.024 | Off |
| □ | 1.507 | Off |
| ◇ | 1.109 | Off |
| △ | 2.024 | On |

(b) $C_{D,i}$ and $w/w_\infty$ plotted against $M$; $\alpha = 0^\circ$.

Figure 39.- Continued.

L-855

Exit-nozzle blisters
○ Off
□ On



(c) $C_{D,i}$ and $w/w_\infty$ plotted against $A_e$; $\alpha = 0^\circ$.

Figure 39.- Concluded.